nutraceuticals

MDPI

Review

Colourimetric Assays for Assessing Polyphenolic Phytonutrients with Nutraceutical Applications: History, Guidelines, Mechanisms, and Critical Evaluation

Joseph Robert Nastasi

School of Agriculture and Food Sustainability, The University of Queensland, Brisbane, QLD 4072, Australia; uqjnasta@uq.edu.au

Abstract

High-throughput colourimetric assays are widely used to screen phenolic phytonutrients in foods and plants, supporting discovery, quality control, and preliminary nutraceutical assessment. This review summarises the historical development, operating principles, and limitations of phenolic-based benchtop methods, and reports practical guidance for defensible application. The following colourimetric approaches are critically evaluated: Folin–Ciocalteu for total phenolics; $AlCl_3$-based and alternative total flavonoid methods; the pH-differential procedure for total monomeric anthocyanins; and tannin assays including vanillin–HCl, butanol–HCl (Porter), DMACA, protein-precipitation, and hydrolysable-tannin (rhodanine/ellagic-acid) protocols. For each method, common biases are identified, matrix interferences, reagent cross-reactivity, oxidative artefacts, dependence on calibration standard, and the chemical meaning of the readout is clarified. A best-practice framework is proposed: define the analytical target; pair complementary assays; pre-clean extracts; justify standards and wavelengths; control oxidation; validate spike-recovery and conversion checks; and contextualise outcomes using functional measures. A consistent conclusion emerges: no single method quantifies "total tannins" or "total flavonoids" across diverse matrices, and transparent reporting with method triangulation is essential for comparability and credible nutraceutical interpretation. The guidance consolidated here aims to standardise practice, minimise over- and underestimation artefacts, and strengthen the evidentiary value of data in food and nutraceutical research.

Keywords: polyphenols; flavonoids; anthocyanins; tannins; nutraceuticals; phytonutrients

check for updates

Academic Editor: Ivan Cruz-Chamorro

Received: 30 September 2025
Revised: 22 November 2025
Accepted: 25 November 2025
Published: 28 November 2025
Corrected: 5 June 2026

Citation: Nastasi, J.R. Colourimetric Assays for Assessing Polyphenolic Phytonutrients with Nutraceutical Applications: History, Guidelines, Mechanisms, and Critical Evaluation. *Nutraceuticals* **2025**, *5*, 40. https://doi.org/10.3390/nutraceuticals5040040

Copyright: © 2025 by the author. Licensee MDPI, Basel, Switzerland. This article is an open access article distributed under the terms and conditions of the Creative Commons Attribution (CC BY) license (https://creativecommons.org/licenses/by/4.0/).

1. Introduction

Plants have long been recognised as a rich source of bioactive compounds that contribute to human health and well-being. Many of these bioactive compounds, collectively termed phytonutrients, are secondary metabolites that plants produce for protection against environmental stressors, pathogens, and omnivores [1]. Unlike essential vitamins and minerals, phytonutrients are not required for basic human nutrition, but they provide health-promoting effects, such as antioxidant, anti-inflammatory, cardioprotective, neuroprotective, and antimicrobial properties [2]. Their presence in fruits, vegetables, herbs, and other plant-based foods has been linked to reduced risks of chronic diseases, including cardiovascular disease, neurodegenerative disorders, and certain cancers [2]. Overall, these attributes underpin the growing recognition of phytonutrients as key nutraceutical candidates, with significant potential for disease prevention and the promotion of long-term human health.

From a nutraceutical perspective, phytonutrients are highly sought after for their ability to support immune function, cognitive health, gut microbiome balance, and metabolic processes [3]. They also play a crucial role in sensory attributes of food such as colour, aroma, and taste, which are key factors in food acceptability, product development, and shelf life [4]. As consumer demand for plant-based, functional foods continues to rise, the need for accurate and high-throughput methods to profile and quantify these bioactive compounds has become increasingly important [5].

Phenolic phytonutrients represent one of the most abundant and functionally diverse groups, classified into distinct subclasses based on their structural motifs and biological activities. Anthocyanins are water-soluble flavonoid pigments that provide red, purple, and blue hues in many fruits and flowers, offering antioxidant, UV-protective, and potential neuroprotective benefits [6]. Curcuminoids, primarily from turmeric, are known for their potent anti-inflammatory and antioxidant effects [7], and vibrant yellow-orange hues. Coumarins, which contribute to the bitter taste of cinnamon and citrus peels, exhibit anticoagulant and antimicrobial properties [8]. Flavonoids and isoflavonoids form one of the largest phytonutrient groups, exhibiting antioxidant, cardiovascular, and antimicrobial benefits, commonly found in tea, citrus fruits, and berries [9]. Lignans and neolignans, abundant in flaxseeds and whole grains, offer oestrogenic and cardiovascular health benefits [10]. Phenolic acids, present in coffee and olives, exhibit antioxidant and anti-inflammatory properties, while tannins, a subset of polyphenols, contribute to the astringency of tea and wine while modulating gut microbiota [11]. Tannins, high–molecular-weight polyphenols formed through the polymerisation of smaller phenolic metabolites, are broadly classified into condensed and hydrolysable types and are known for their strong protein-binding capacity, antioxidant activity, and emerging roles in cardiometabolic and gut health [11–14]. Together, these phenolic phytonutrient classes not only shape the sensory qualities of plant-based foods but also underpin their positioning as key candidates for the development of next-generation nutraceuticals and functional foods.

Among the various analytical techniques available, high throughput colourimetric assays have emerged as indispensable tools for the rapid screening of phytonutrient classes in foods and plants. These assays rely on specific chemical reactions that produce measurable colour changes, providing a cost-effective and scalable approach for qualifying and quantifying key bioactive compounds [15]. Unlike chromatographic techniques, which require specialised instrumentation and complex sample preparation, colourimetric methods offer simplicity, speed, and accessibility, making them widely used in both research and industrial settings [16].

Despite their widespread application, several methodological challenges must be addressed to ensure the accuracy, reliability, and reproducibility of colourimetric assays. Many assays lack specificity, often reacting with multiple structurally similar compounds within the same class, leading to potential over- or underestimation of true phytonutrient content [15]. Variations in solvent composition, reaction conditions, reagent stability, and detection wavelengths can introduce inconsistencies, making direct comparisons between studies difficult [17]. Another key challenge is the selection of reference standards, for example, flavonoid content via benchtop assay determination is frequently reported as quercetin equivalents, even when quercetin is not the predominant flavonoid in the sample, leading to discrepancies in quantification [18]. Addressing these limitations requires standardised methodologies, appropriate controls, and a critical understanding of each assay's strengths, limitations, and scientific basis. Due to their easy-to-follow methods, these key aspects of quality control are often overlooked.

Given the extensive use of high-throughput colourimetric assays in food and nutraceutical research, it is critical to establish best practices for their implementation and

interpretation. Previous reviews have largely summarised assay chemistry and reagent performance, but few have translated this information into laboratory decision-making frameworks. This review improves usability by providing a bench-oriented, practice-focused comparison of widely used colourimetric methods for phenolic phytonutrient analysis. This review emphasises how specific methodological choices directly influence assay accuracy and comparability across laboratories. A critical assessment of specificity, interferences, and standardisation challenges of major assays is presented alongside practical recommendations for reproducible quantification. Together, these elements provide a reference guide for both academic and nutraceutical QA/QC laboratories, offering not only an evaluation of existing methods but also a decision framework to support evidence-based assay selection and reporting.

2. UV Absorption Properties of Phenolic Compounds

Phenolic phytonutrients exhibit distinctive spectroscopic signatures that enable their detection and quantification using benchtop UV–Vis spectrophotometric assays. The UV spectrum spans 100–400 nm, the visible range extends from 400–800 nm, and together these form the ultraviolet–visible (UV–Vis) region (100–800 nm) for phenolic compounds. Within this region, phenolic compounds display characteristic UV–Vis patterns due to their conjugated double bonds and aromatic ring structures, making UV–Vis spectroscopy an indispensable screening tool for their rapid assessment in foods and plants [19–22].

For flavonoids, which possess a C6–C3–C6 backbone with two interacting chromophores, two characteristic absorption regions are typically observed:

- Band II (240–280 nm), associated with the benzoyl system of ring A.
- Band I (300–380 nm), associated with the cinnamoyl system of ring B.

It is important to note that the assignment of Band I and Band II is not entirely consistent across the literature. While some papers invert the numbering, the convention most widely accepted in flavonoid spectroscopy—including authoritative texts by Harborne and Mabry [21]—defines Band II (240–280 nm) as the benzoyl system of ring A and Band I (300–380 nm) as the cinnamoyl system arising from ring B and the conjugated C-ring. The present review adopts this modern and widely applied convention, which also underpins contemporary HPLC–DAD and LC–UV workflows for flavonoid identification. By contrast, some important and recent computational or spectroscopic studies, such as Gierschner, et al. [23] use the opposite numbering scheme and cite classical flavonoid texts [20–22] as justification; however, those original sources do not support the inverted assignment, contributing to ongoing inconsistency in the field.

The precise wavelength maxima (λ_{max}) of phenolic compounds depend on hydroxylation, glycosylation, and substitution patterns on the aromatic rings. Increased hydroxylation generally causes bathochromic shifts (longer λ_{max}), whereas methylation tends to stabilise the chromophore and can produce hypsochromic shifts [23]. These shifts originate from changes in molecular conjugation, where alternating double bonds allow π-electrons to delocalise across the structure. When UV–Vis light provides energy matching the gap between the ground (π) and excited (π) states, these electrons are promoted to higher energy levels, and increasing conjugation lowers this energy gap, shifting absorption toward longer wavelengths [23]. Flavonoids share a common C6–C3–C6 backbone (2-phenyl-1,4-benzopyrone), with UV absorption shaped by the number and position of hydroxyl groups on the A and B rings [23]. For example, some major subclasses exhibit distinct features:

- Flavonols and flavones: strong absorption around 350 nm due to extensive conjugation.
- Flavanones and flavanols: weaker or shifted Band I absorption owing to reduced conjugation.

- Isoflavonoids: shifts in Band I absorption due to relocation of the B ring to the C3 position, altering resonance.
- Anthocyanins: unique visible absorption at ~520 nm due to the positively charged flavylium cation, responsible for their vivid red, purple, and blue pigmentation.

Phenolic acids are structurally simpler to flavonoids but still informative. Hydroxybenzoic acids (e.g., gallic acid) exhibit maxima at ~280 nm due to ring hydroxylation, while hydroxycinnamic acids (e.g., caffeic, ferulic acids) display additional absorption between 300–360 nm, attributed to conjugated double bonds in the side chain [24].

To assist users in understanding absorption patterns of phenolic compounds a simplified classification framework is displayed in Figure 1. Figure 1 depicts the regions of some phenolic acids and flavonoids that impact absorption behaviour and the role of conjugation and hydroxyl substitution in spectral behaviour. For example, catechin (a flavanol or flavan-3-ol) exhibits strong absorbance at 280 nm and doesn't absorb at 340–370 nm because its flavanol structure lacks the C2=C3 double bond and 4-ketone needed for extended conjugation, so it cannot generate the long-wavelength Band I typical of flavonols or flavones. Quercetin, (a flavonol) presents both Band II (~260 nm) and Band I (~370 nm) characteristics because it possesses a C2=C3 double bond and a 4-ketone, allowing full conjugation between the B-ring and the central heterocycle, which enables the longer-wavelength $\pi \rightarrow \pi^*$ transition associated with Band I. Anthocyanins, by contrast, absorb well into the visible range because the flavylium cation features an extensively conjugated π-electron system spanning all three rings, together with a positively charged heterocycle that further stabilises long-wavelength electronic transitions. This results in strong absorbance maxima around ~520 nm, which directly corresponds to the red–purple–blue hues observed in pigmented fruits and flowers [25].

From a nutraceutical perspective, these UV–Vis properties provide more than analytical convenience, they also underpin the use of colourimetric assays that rely on absorbance shifts to estimate phenolic-related content in complex plant and food extract matrices. Moreover, the same structural features that determine spectral behaviour, conjugation, hydroxylation, and glycosylation, are also central to bioactivity, influencing antioxidant capacity, metal chelation, and interactions with biomolecules [26]. Although not explicitly depicted in Figure 1, tannins also conform to these principles. For example, condensed tannins (proanthocyanidins) are polymers of catechin and epicatechin and therefore exhibit strong absorbance around 280 nm, with spectral broadening as polymer size increases [13,27]. Hydrolysable tannins, such as gallotannins and ellagitannins, reflect the spectral features of their constituent phenolic acids, typically with maxima at 280 nm for gallic acid and additional bands for ellagic acid derivatives [28]. Phlorotannins, by contrast, are composed of polymerised phloroglucinol units, typically showing strong absorbance between 260–280 nm with broader featureless spectra as polymer length increases [29]. Because tannins amplify rather than introduce unique spectral signatures, they are generally interpreted through the absorption properties of their monomeric units.

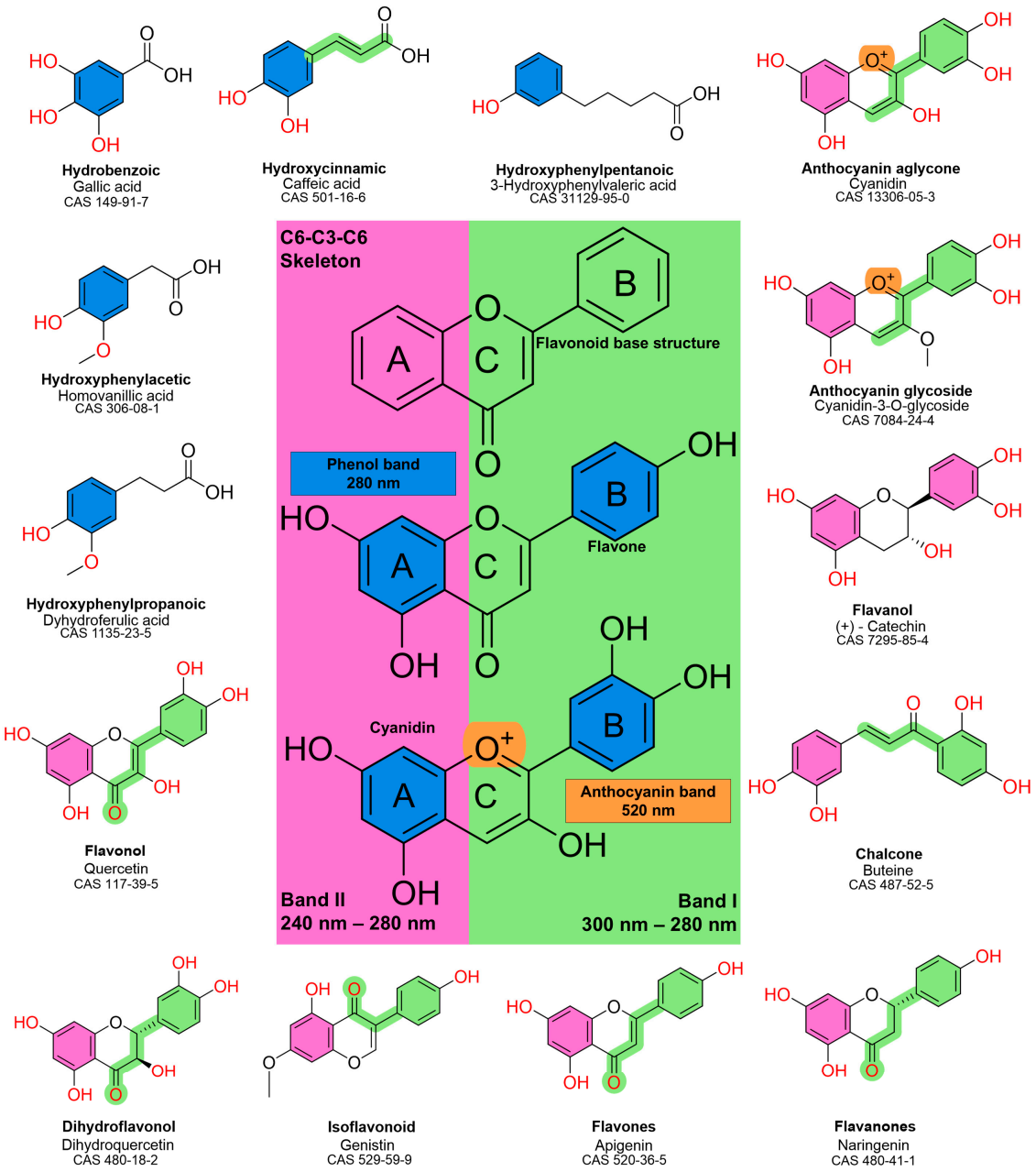


Figure 1. UV–VIS–relevant structural features of phenolic acids, flavonoids, and anthocyanins. Representative phenolic acids (**top left**) illustrate the generic phenolic chromophore (blue highlight), responsible for the ~280 nm band common to all phenols, with hydroxycinnamic acids additionally showing extended conjugation (green highlight) that produces absorption around 320–350 nm. The central C6–C3–C6 flavonoid skeleton highlights Band II (240–280 nm) arising from the A-ring benzoyl system (pink highlight) and Band I (300–380 nm) from the B-ring cinnamoyl system (green). Surrounding flavonoid subclasses illustrate how saturation and substitution alter λ_{max}, with red hydroxyl groups emphasising their electron-donating influence on band shifts. Anthocyanidins and their glycosides (**top right**) feature the flavylium cation (orange highlight), which generates the characteristic ~520 nm visible band associated with red–purple pigmentation. This figure presents a visual guide for understanding UV absorption patterns but is not developed from experimental data, therefore, true absorbance regions will vary slightly.

3. The Role of High-Throughput Colourimetric Assays

High-throughput analysis refers to analytical methods designed to rapidly process a large number of samples with minimal hands-on time, making them suitable for screen-

ing applications in food, nutraceutical, and plant-based research [30]. In the context of benchtop colourimetric assays, high-throughput capabilities are defined by several key factors, including sample processing speed, automation potential, scalability, and data reproducibility [31].

Given the structural complexity and functional diversity of phytonutrients, accurate quantification and classification are essential for understanding their biological roles and nutraceutical potential. High-throughput colourimetric assays are among the most widely used techniques for phytonutrient analysis because they are:

- Rapid and cost-effective: High-throughput colourimetric assays are capable of processing numerous samples within a relatively short timeframe, making them ideal for large-scale screening studies. Their low operational costs contribute to their widespread application, particularly in settings where budget constraints are a consideration.
- Accessible: Unlike more sophisticated analytical techniques that require expensive instrumentation, high-throughput colourimetric assays can be performed using basic spectrophotometric equipment. This accessibility allows researchers across various fields to apply these methods without significant financial or technical barriers.
- Versatile: The adaptability of colourimetric assays makes them suitable for analysing a wide range of sample types, including plant extracts, food matrices, and nutraceutical formulations. The flexibility of these assays also allows modifications to enhance specificity, sensitivity, or throughput, depending on the analytical requirements.

The two standard protocols for implementing high-throughput benchtop assays involve the use of either cuvettes or well-plates (microplates) (Figure 2). Cuvette-based assays are typically employed for single-sample measurements, offering high accuracy but limited throughput. In contrast, well-plate assays, particularly those conducted using 96-well or 384-well plates, provide the capacity to simultaneously process multiple samples under identical conditions, significantly enhancing throughput and reproducibility. Furthermore, the integration of automated liquid handling systems with well-plate assays allows for even greater efficiency and consistency, making them highly attractive for screening and comparative studies in phytonutrient research [32].

3.1. General Guidelines for Colourimetric Assays

Despite their advantages, colourimetric assays also have limitations related to specificity, reagent stability, and inter-laboratory variability. Many colourimetric methods provide total content estimations rather than precise quantification of individual compounds, leading to potential inaccuracies if not properly standardised [15]. Therefore, establishing best practices for their application is critical for ensuring reproducibility and meaningful interpretation of results.

General guidelines for colourimetric assays involve optimising various parameters to ensure reliable and accurate measurements. First, selecting the appropriate wavelength corresponding to the λ_{max} of the coloured species is essential for sensitivity and accuracy. This is important as laboratory conditions can deviate the λ_{max} from the recommended values of published methods. For pH-dependent assays, such as those involving anthocyanins, measurements are taken at different pHs to capture relevant spectral shifts [33]. Furthermore, calibration curves must be prepared using known concentrations of the target compound to establish a reliable linear response range. Measuring samples within the absorbance range of 0.1–1.0 ensures maximum accuracy [34], however, modern spectrophotometric systems provide linearity beyond 1.0. Reagents should be freshly prepared, when possible, as degradation over time can impact colour responses, and adequate storage conditions should be maintained to ensure stability. Additionally, samples should be prepared to fall

within the linear range, with filtration or centrifugation used to remove particulate matter that could interfere with absorbance readings.

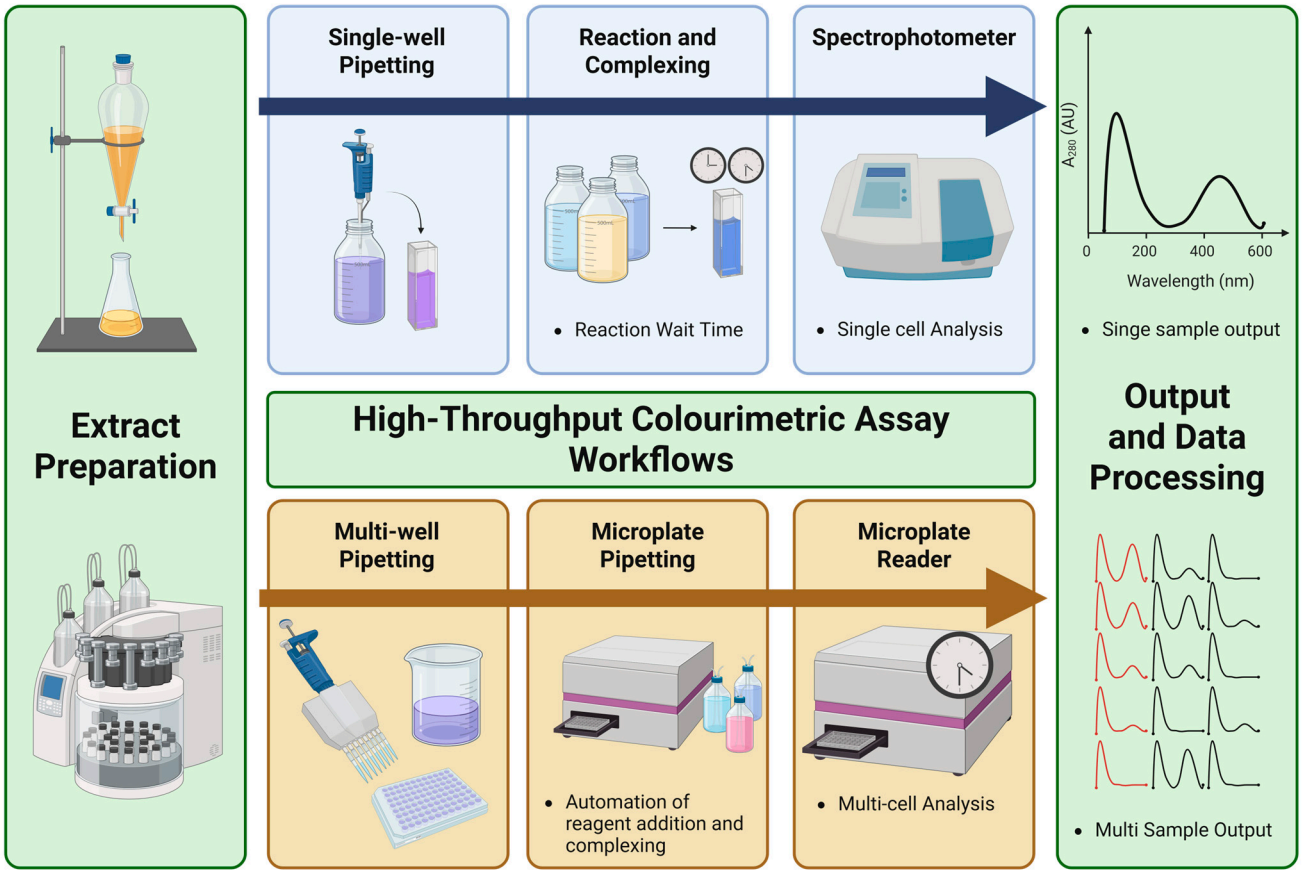


Figure 2. Workflow comparison of conventional and high-throughput colourimetric assays. Schematic representation of extract preparation, assay setup, and data acquisition using single-sample cuvette-based protocols (**top**) versus high-throughput well-plate workflows (**bottom**). Conventional single-well approaches involve manual pipetting, reaction complexing, and spectrophotometric measurement, providing single-sample output. High-throughput workflows employ multi-well pipetting and microplate readers, often coupled with automated reagent handling, enabling parallel processing and multi-sample output with improved reproducibility and efficiency.

Path length considerations are critical, particularly when using microplate-based assays where shorter path lengths require appropriate calibration or correction factors [35]. Interfering substances present in complex matrices, such as plant extracts or food samples, can influence absorbance measurements. Therefore, appropriate blanks, including reagent and solvent blanks, should be used to account for background absorbance [36]. Maintaining consistent reaction conditions, including temperature, pH, and ionic strength, is also necessary to ensure reproducibility. These environmental conditions are often easier controlled in microplate readers compared to single cuvette spectrophotometers [32]. To improve accuracy, measurements should be performed in triplicate at a minimum. Proper documentation of protocols, including reagent concentrations, reaction times, and wavelengths, is essential for reproducibility and comparability across studies. Colourimetric assays are based on the principle of light absorbance and transmittance as they pass through a solution, governed by the Beer-Lambert Law. This law describes the relationship between the attenuation of light and the concentration of absorbing compounds within a solution. It is important that a basic understanding of the Beer-Lambert law be known to any user when conducting colourimetric assays so that potential errors can be troubleshooted effectively.

3.2. Beer-Lambert Law, Absorbance Measurements, and the Spectrophotometer

The Beer–Lambert Law provides the theoretical basis for spectrophotometric quantification. It describes a linear relationship between absorbance (A) and the product of the molar absorption coefficient (ε), the analyte concentration (c), and the optical path length (l) of the cuvette according to Equation (1):

$$A = \varepsilon cl \tag{1}$$

Absorbance is a logarithmic measure of light attenuation relative to incident intensity (I_0) and transmitted intensity (I), expressed as Equation (2):

$$A = log_{10}\frac{I_0}{I} = -log_{10}T \tag{2}$$

where T is the transmittance (I/I_0).

By definition, an absorbance of 0 corresponds to 100% transmittance, while an absorbance of 1 corresponds to 10% transmittance [34,37,38]. This logarithmic scaling makes the absorbance axis convenient, because under ideal conditions it is directly proportional to the analyte concentration.

Spectrophotometers apply the Beer–Lambert principle by separating white light into discrete wavelengths using a monochromator, typically a diffraction grating, and directing the selected wavelength through a cuvette containing the sample. The detector measures the transmitted light intensity, compares it to the incident light, and reports the absorbance value. As illustrated in Figure 3, the light source, grating, sample compartment, and detector components are shown within a simplified optical pathway that visualises how absorbance is physically generated.

In colourimetric phenolic assays, wavelength selection is critical. Phenolic acids and flavonoids exhibit strong intrinsic absorbance due to aromatic π–π* transitions [23], but colourimetric methods rely on derivatisation reactions that produce stable chromophores with distinct absorption maxima in the visible region. For example, Folin–Ciocalteu products are read at 765 nm [39]. By targeting these characteristic maxima, the spectrophotometer provides sensitive and selective quantification of phenolic content in complex plant extracts.

3.3. Well Plate (Microplate) Path-Length Correction Guide

Microplate spectrophotometry offers rapid throughput and reduced reagent use, yet the short and variable optical path length in wells introduces systematic error if untreated. Because most colourimetric assays were originally standardised for a 1 cm cuvette geometry, absorbances measured in 96- or 384-well plates must be either normalised to an equivalent 1 cm path or calibrated directly in the same microplate conditions. A brief example is provided to estimate pathlength correction when the in-built feature is not available in the instrument software. Measure the absorbance of pure water in the same well at ~977 nm and optionally subtract a baseline at ~900 nm and determine the baseline-corrected water signal according to Equations (3) and (4):

$$A^*_{977} = A_{977} - A_{900} \tag{3}$$

Effective path length in the well (cm), referenced to a 1 cm cuvette of water:

$$l_{well} = \frac{A^*_{977,\text{well}}}{A^*_{977,\text{cuvette}}} \times 1\ \text{cm} \tag{4}$$

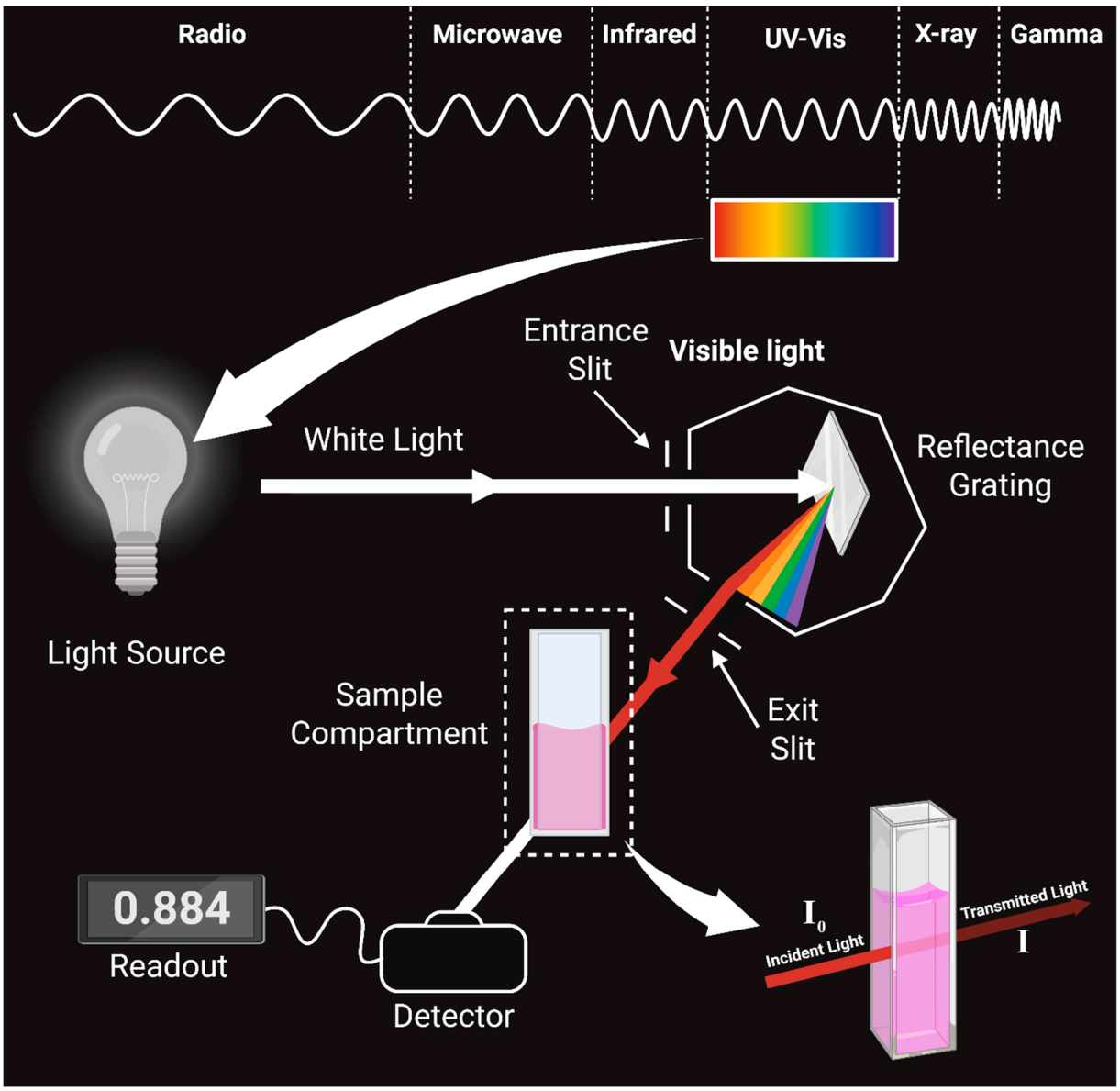


Figure 3. Simplified diagram of a UV spectrophotometer operating under a single wavelength. White light is dispersed by a diffraction grating, and a selected wavelength is passed through the cuvette. The detector compares transmitted intensity (I) with the incident beam (I_0) to calculate absorbance, which is displayed as the digital readout.

4. Major Colourimetric Methods for Phenolic-Based Phytonutrient Classes

4.1. Polyphenols and Phenol Ring Containing Compounds

The polyphenolic metabolome of foods and plants encompasses several major classes, each with distinct structural and functional characteristics [40]. Flavonoids represent the largest group, comprising various subclasses such as anthocyanins, chalcones, dihydrochalcones, dihydroflavonols, flavanols, flavanones, flavones, flavonols, and isoflavonoids. The phenolic acids group includes hydroxybenzoic acids, hydroxycinnamic acids, hydroxyphenylacetic acids, and hydroxyphenylpropanoic acids. These molecules, derived mainly from the shikimic acid pathway, play essential roles in plant defence, flavour development, and antioxidant capacity [41]. Stilbenes and lignans form smaller but bioactive classes, both containing phenylpropanoid-derived structures [42]. Other polyphenolic subgroups include a diverse range of less abundant but chemically significant categories such as alkyl-

methoxyphenols, alkylphenols, curcuminoids, furanocoumarins, hydroxybenzaldehydes, hydroxybenzoketones, hydroxycinnamaldehydes, hydroxycoumarins, hydroxyphenylpropenes, methoxyphenols, naphthoquinones, phenolic terpenes, and tyrosols [43]. All together, these compounds share a unifying chemical feature which is the presence of one or more phenolic hydroxyl groups attached to an aromatic ring. The electron-donating ability of the hydroxyl group and it subsequent reducing power underpins their antioxidant potential and also forms the basis for their quantification through colourimetric assays such as the Total Phenolic Content (TPC) protocol. A hierarchical breakdown of some of the major phenolic subclasses and related compounds are visualised in Figure 4.

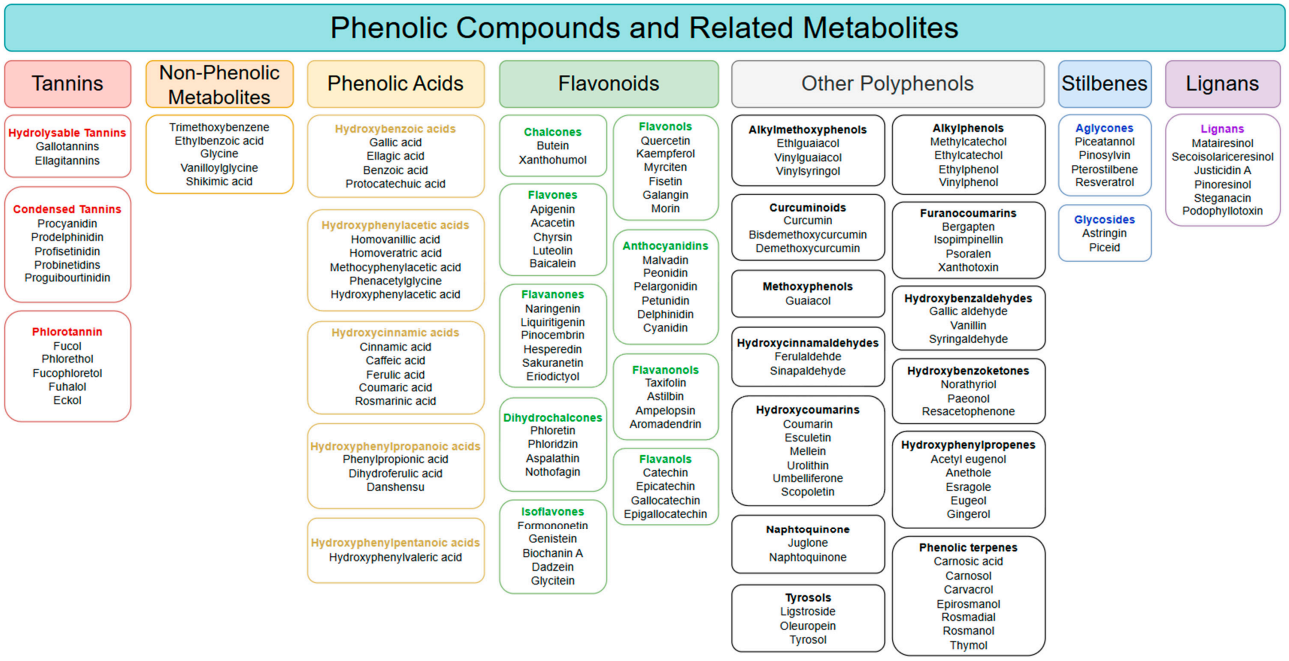


Figure 4. This figure summarises the hierarchical relationships among phenolic compounds, grouped into their primary structural families: tannins, phenolic acids, flavonoids, other polyphenols, stilbenes, and lignans. Subclasses are organised according to shared core scaffolds (e.g., hydroxybenzoic acids, chalcones, flavonols, coumarins), with representative compounds listed beneath each category. Non-phenolic metabolites commonly co-occurring in plant extracts are included to highlight structurally related molecules that contribute to extract complexity but do not possess a phenolic ring.

4.1.1. TPC Assay Overview and Historical Context

Quantification of polyphenols is commonly performed using the TPC assay, which employs the Folin-Ciocalteu (F–C) reagent in a redox reaction that produces a measurable colour change. Originally developed by Folin and Ciocalteu [44] to measure tyrosine and tryptophan in proteins, the assay was later adapted for phenolic quantification due to the F–C reagent's ability to react with phenolic hydroxyl groups, forming a blue complex measurable at 765 nm [45]. Singleton and Rossi [45] refined the method specifically for plant extracts, wines, and food samples, establishing its widespread use in food science and phytochemistry. Further improvements by Ainsworth and Gillespie [46] standardised the protocol for plant tissue analysis, optimising reagent concentrations and sample preparation for greater accuracy. More recently, Everette, et al. [47] conducted a comprehensive evaluation of the F–C reagent's reactivity, identifying potential interferences from non-phenolic reducing agents, while Sánchez-Rangel, et al. [48] introduced specificity enhancements to improve reliability. These refinements have led to the modern, mainstream version of the F–C assay, which remains the gold standard for high-throughput TPC determination in food, plant, and nutraceutical research.

4.1.2. Folin-Ciocalteu Standard Procedure for TPC

The F–C assay for TPC determination follows a standardised procedure based on a redox reaction between phenolic compounds and the F–C reagent. First, sample extracts containing phenolics are prepared using solvents such as methanol, ethanol, acetone, or water, followed by filtration or centrifugation to remove solid residues and higher molecular weight polymers. The assay begins with the addition of the F–C reagent, typically diluted 1:10 with distilled water, to a fixed volume of the sample. After 5 min, a sodium carbonate (Na_2CO_3) solution (7–10%) is added to adjust the pH, facilitating the reduction of Mo^{6+} to Mo^{5+}, leading to the formation of a blue-coloured complex. It is recommended at this point that readers review the specificity improvements suggested by Sánchez-Rangel, et al. [48] to overcome the limitations imposed by the interferences of other reducing compounds present in crude plant extracts that can lead to inflated TPC values. The reaction mixture is then incubated at room temperature or 40 °C for 30–120 min, allowing for full colour development. Absorbance is measured at 765 nm using a UV–Vis spectrophotometer, with higher absorbance indicating a greater phenolic content. Quantification is performed using a calibration curve, with gallic acid as the most commonly used standard due to its high purity, solubility, and stable reactivity. Results are expressed as Gallic Acid Equivalents (GAE) per gram or mL of extract (mg GAE/g or mg GAE/mL), enabling standardised comparisons across different samples. While other phenolic standards such as catechin, chlorogenic acid, and tannic acid can be used, gallic acid remains the universal reference in food, plant, and nutraceutical research due to its consistent reactivity with the F–C reagent.

4.1.3. Mechanistic Basis of Colour Development in the TPC Assay

At the mechanistic level, the TPC assay reaction pathway that underpins colour development can be understood as follows: Under alkaline conditions, phenolic hydroxyl groups (Ar–OH) are deprotonated to form phenolate anions ($Ar–O^-$), which act as electron donors [39], where Ar is aryl group, which is a general representation for an aromatic ring system. These anions undergo oxidation, producing semiquinone or quinone structures, while simultaneously transferring electrons to the Mo^{6+} and W^{6+} centres of the F–C reagent [39]. This electron transfer reduces Mo^{6+} and W^{6+} to their lower valence states (Mo^{5+}/W^{5+}), generating mixed-valence heteropoly complexes with a blue hue [39]. These complexes are responsible for the characteristic absorption at ~760–765 nm. The overall process can be summarised as follows or visualised stepwise in Figure 5 using gallic acid as the compound under oxidation.

1. Deprotonation: $Ar–OH + OH^- \rightarrow Ar–O^- + H_2O$
2. Oxidation of phenolics: $Ar–O^- \rightarrow Ar=O$ (quinone/semiquinone) + e^-
3. Reduction of F–C reagent: $Mo^{6+}/W^{6+} + e^- \rightarrow Mo^{5+}/W^{5+}$
4. Complex formation: Reduced heteropoly acids assemble into blue-coloured mixed-valence complexes measurable spectrophotometrically.

4.1.4. Specificity, Interpretation, and Complementary Methods for Phenolic Content

It is important to mention that due to the non-specific nature of the TPC assay, chromatographic techniques such as High-Performance Liquid Chromatography with Diode-Array Detection (HPLC-DAD) and Liquid Chromatography-Tandem Mass Spectrometry (LC-MS/MS) provide superior specificity by identifying and quantifying individual phenolic compounds [49]. In addition, spectroscopic methods, including Fourier Transform Infrared Spectroscopy (FTIR) and full spectrum UV–Vis Spectroscopy, are also employed for phenolic fingerprinting and rapid screening [50], and when coupled with chemometric analysis techniques, powerful correlation and discrimination models may be generated to rapidly screen samples [51].

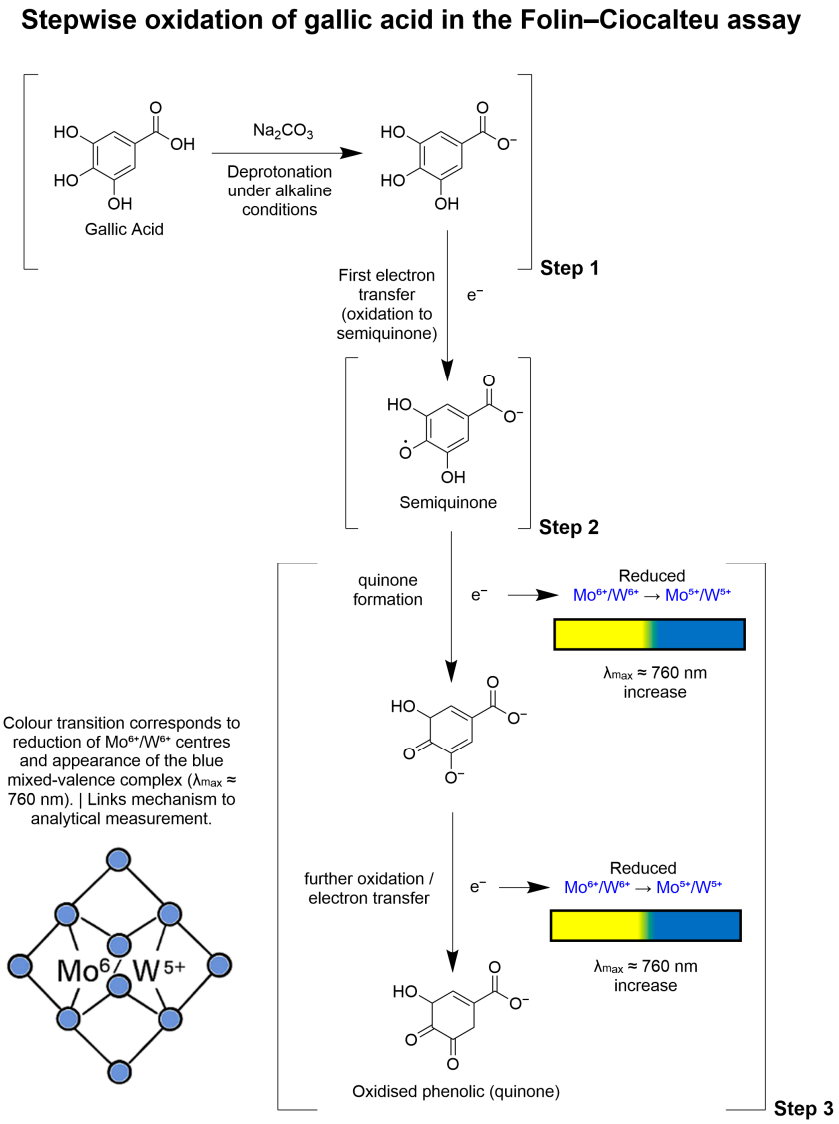


Figure 5. Shortened stepwise oxidation of gallic acid in the Folin–Ciocalteu (F–C) assay. Under alkaline conditions (Na_2CO_3), gallic acid undergoes deprotonation to form a phenolate anion capable of electron donation to the phosphomolybdic/phosphotungstic heteropoly acids in the (F–C) reagent. Sequential single-electron transfers yield first a semiquinone radical intermediate, followed by oxidation to a quinone. Each electron transfer reduces the molybdenum and tungsten centres ($Mo^{6+}/W^{6+} \rightarrow Mo^{5+}/W^{5+}$), generating the characteristic blue mixed-valence heteropoly complex responsible for the absorbance maximum at approximately 760 nm. The accompanying colour transition from yellow to blue illustrates the analytical basis of the total phenolic content (TPC) assay. Mechanistic steps shown are schematic representations intended to illustrate likely reaction pathways in TPC assay conditions; they are not drawn as full electron-pushing mechanisms.

4.1.5. Comparison of Benchmark Parameters for TPC Determination

The comparative benchmark data summarised in Table 1 highlight the analytical equivalence and operational advantages between the conventional cuvette-based F–C assay [52] (AOAC Official Method 2017.13) and its 96-well microplate adaptation [53]. Both methods are based on the same electron-transfer reduction of Mo^{6+}/W^{6+} to Mo^{5+}/W^{5+}, forming a blue heteropoly complex indicative of phenolic-like reducing capacity. Despite the significant miniaturisation of volumes in the microplate format, the results demonstrate comparable precision, linearity, and recovery across a wide calibration range when expressed as GAE.

Table 1. Comparative benchmark parameters for Total Phenolic Content (TPC) determination using the Folin–Ciocalteu assay in cuvette and 96-well microplate formats.

Method	Conventional Cuvette Method (AOAC Official Method 2017.13)	96-Well Microplate Method
Reference	[52]	[53]
Assay name	TPC determined by F–C assay; results expressed as mg GAE g^{-1} or mg L^{-1}	TPC determined by F–C assay; microplate adaptation; mg GAE g^{-1} or mg L^{-1}
Reaction principle	Electron-transfer reduction of Mo $Mo^{6+}/W^{6+} \rightarrow Mo^{5+}/W^{5+}$; blue heteropoly complex formation (phenolic-like reducing capacity)	Identical reaction; miniaturised volumes and optical path for high-throughput quantification
λ_{max} (nm)	765 nm	750–765 nm (absorbance window can be higher if filters are used)
Sample/reagent setup	1 mL extract + 1 mL F–C → 6 min → + 3 mL 20% Na_2CO_3 w/v → 120 min at 30–40 °C → read 765 nm	20 µL extract + 100 µL F–C (1:4) → shaken for 60 s → stand 240 s → + 75 µL Na_2CO_3 w/v (100 g L^{-1}) → shake 1 min → 2 h at room temperature → read 750 nm
Calibration range/model	40–200 mg L^{-1} GAE (5 points: 40, 80, 120, 160, 200); linear through origin; $r^2 \geq 0.990$ (observed 0.996–1.000); y = 0.00572x (± 0.00021) + 0.0261 (± 0.0266).	10–200 mg L^{-1} GAE; r^2 = 0.9998; y = 0.0076x + 0.0109
LOD/LOQ	LOQ = 40 mg L^{-1} GAE (solution); extract range ≈ 5–100% w/w	LOD = 0.74 mg L^{-1}; LOQ = 2.24 mg L^{-1} GAE
Linearity/method equivalence	Meets AOAC SMPR criteria; linear forced through zero	Statistically equivalent to cuvette method (slope 0.966–0.998; $p > 0.05$)
Precision (RSDr)	Within-day 1.96–6.38%; between-day ≤ 13.77%; total ≤ 15.18% (matrix-dependent)—meets SMPR > 5 mg L^{-1}	Repeatability ≤ 3.6%; reproducibility ≤ 6.1% (intra-lab)
Accuracy (recovery)	91–104% (GA spikes in maltodextrin 30–70% w/w)	87.8–100.3% (GA spikes 12–60 mg L^{-1})
Ruggedness/robustness	No significant effect from variations in apparatus; test-portion 100 vs. 200 mg; read 0 vs. 15 min; F–C 1 vs. 2 mL; reaction 90 vs. 120 min; 30 vs. 40 °C; Na_2CO_3 2 vs. 3 mL	No bias vs. cuvette (F- and *t*-tests $p > 0.05$ across ranges)
Selectivity/interferences	Responds to reducing species (phenolics, ascorbate, amino acids); no positive interference from ≤1 mg mL^{-1} glucose, fructose, sucrose	Same; recommend PVPP or SPE cleanup for sugar/ascorbate-rich matrices
Preferred standard and expression	Gallic acid (≥98%); report mg GAE g^{-1} extract (dry basis) or % w/w	Gallic acid (≥98%); report mg GAE g^{-1} or mg L^{-1} extract
Compliance with AOAC SMPR 2015.009	Meets criteria (80–110% recovery; RSDr ≤ 7%; linear 5–500 mg L^{-1} GAE verified 40–200)	Meets and exceeds precision and throughput requirements
Throughput/reagent use	Single-sample workflow; large volumes (~5–10 min pipetting per sample)	96 samples per run; ≈ 20 × lower reagent volume; ≈ 12 × higher throughput
Terminology/best practice	Use "Total Phenolic Content (TPC)" throughout; acknowledge measurement reflects phenolic-like reducing capacity; include matrix blank and spike-recovery controls	Same; apply path-length correction or plate-specific calibration curve for absorbance normalisation

Summary of key analytical performance parameters of the Folin–Ciocalteu (F–C) assay in conventional and microplate configurations. Both rely on Mo^{6+}/W^{6+} reduction to Mo^{5+}/W^{5+} blue heteropoly complexes at ~765 nm, expressing results as gallic acid equivalents (GAE). Data reflects cited validation studies without re-normalisation. Abbreviations: GAE, gallic acid equivalent; LOD, limit of detection; LOQ, limit of quantification; RSDr, relative standard deviation of repeatability; SMPR, Standard Method Performance Requirement (AOAC 2015.009). Matrix blanks, spike-recovery checks, and plate-specific calibration corrections are recommended best practices. → symbol indicates the sequential step in the assay method.

As shown in Table 1, the microplate approach achieves near-identical analytical performance ($r^2 \approx 0.999$, recovery ≈ 88–100%) while reducing reagent consumption by more than an order of magnitude and enabling a throughput exceeding 90 samples per run. Importantly, both methods satisfy AOAC SMPR 2015.009 acceptance criteria for linearity, precision, and accuracy, confirming that the microplate configuration does not compromise analytical quality. Minor procedural differences such as path-length normalisation, shorter incubation times, and automated pipetting should nonetheless be reported explicitly to ensure reproducibility.

The benchmark comparison further reinforces that F–C values represent a reducing-capacity index rather than a structurally selective quantification of total phenolics. Accordingly, the use of consistent terminology ("Total Phenolic Content–TPC") and transparent calibration referencing (mg GAE g^{-1} DW or mg GAE L^{-1}) is essential to facilitate cross-study comparison.

4.2. Flavonoids

4.2.1. Overview and Presence in Different Nutraceutical Foods

Flavonoids are a distinct subclass of the polyphenol family characterised by a 15-carbon skeleton and a common C6–C3–C6 backbone, consisting of two aromatic rings linked by a three-carbon bridge (Figure 6). Their structural diversity influences their antioxidant, anti-inflammatory, and UV-protective properties, making them valuable in nutraceutical and cosmetic applications [54].

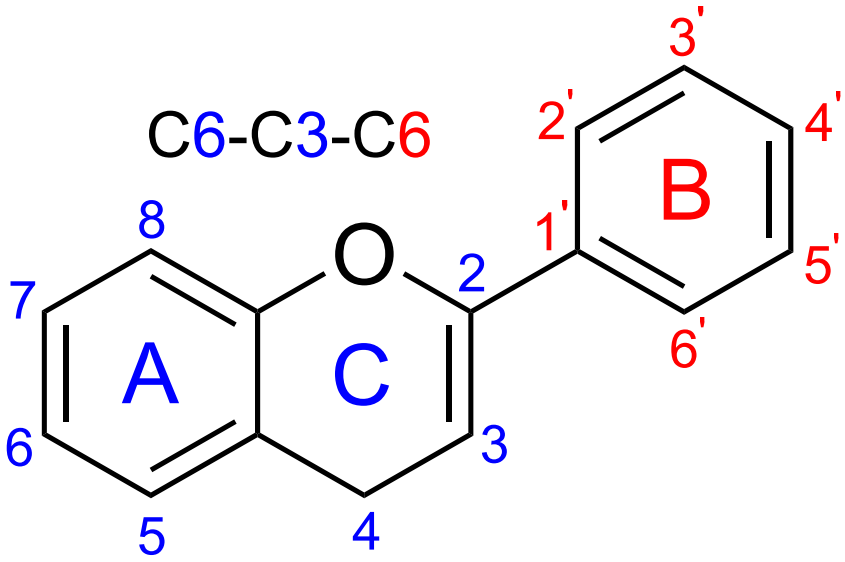


Figure 6. Core flavonoid skeleton (C6–C3–C6) showing the arrangement and numbering of the A, B, and C rings. Rings A and B represent the two aromatic systems, while the heterocyclic C ring bridges them through a three-carbon linkage. This backbone serves as the fundamental structural framework for all flavonoid subclasses (e.g., flavanols, flavanones, flavones, flavanonols, isoflavones, and anthocyanins), with variations in oxidation state and substitution patterns on each ring determining the compound's subclass and bioactivity.

The six principal subclasses of flavonoids— flavonols (3-hydroxyflavones), flavones, flavanones (dihydroflavones), flavanonols (dihydroflavonols or 3-hydroxyflavanones), flavanols (flavan-3-ols or catechins), and isoflavones—are shown in Figure 7, alongside representative molecular structures and natural food sources of notable nutraceutical activity displayed in Table 2. These subclasses share the same fundamental flavone backbone but differ in oxidation and substitution patterns on the A, B, and C ring, producing distinct chromatic and bio-functional profiles in different nutraceutical contexts [55–57]. This structural variability underpins the broad range of biological activities and spectrophotometric behaviours observed across flavonoid assays. Moreover, these structures represent the aglycone forms, whereas in plants, flavonoids predominantly occur as glycosides conjugated with sugars such as glucose, rhamnose, or rutinose [58]. Glycosylation increases solubility and stability, enabling efficient storage and transport within plant tissues, and also modifies biological availability, intestinal absorption, and metabolic turnover in humans [59]. Consequently, the balance between aglycone and glycosylated forms plays a critical role in determining the bio-efficacy of flavonoids as nutraceuticals, influencing both their in-vivo antioxidant performance and their potential for targeted health applications [58].



Figure 7. Flavonoids comprise six principal subclasses—flavonols, flavones, flavanones, flavanonols, flavanols, and isoflavones—each sharing the common C6–C3–C6 flavone backbone but differing in the oxidation state and substitution pattern of the heterocyclic (C) ring. Representative molecular structures are shown alongside characteristic plant or fruit sources. Colour grouping reflects subclass differentiation: flavonols (yellow), flavones (cream), flavanones (orange), isoflavones (violet-pink), flavanonols (green), and flavanols (brown). In nature, these aglycones typically occur as glycosides conjugated with mono- or disaccharides, affecting not only solubility and pigment localisation but also bioavailability and metabolic fate in humans—key determinants of their nutraceutical potential.

Table 2. Food Sources of different flavonoid aglycones from the major flavonoid subclasses.

Subclass	Aglycone	Food Sources	Reference
Flavanones	Liquiritigenin	*Glycyrrhiza uralensis* (licorice), *Artocarpus heterophyllus* (jackfruit)	[60]
	Pinocembrin	*Boesenbergia rotunda* (fingerroot), honey, *Litchi chinensis* (lychee seeds)	[61,62]
	Hesperidin	*Mentha* × *piperita* (peppermint), *Citrus paradisi* (grapefruit), *Citrus* × *limon* (lemon)	[63]
	Sakuranetin	*Citrus* × *sinensis* (orange), *Oryza sativa* (rice), *Piper lanceifolium*	[64]
	Eriodictyol	*Citrus* × *limon*, *C. paradisi*, *C.* × *aurantiifolia* (lime)	[65]
	Naringenin	*Citrus paradise* (Grapefruit), *Prunus* spp. (Cherries), *Solanum lycopersicum* (Tomatoes)	[66]

Table 2. *Cont.*

Subclass	Aglycone	Food Sources	Reference
Flavones	Apigenin	*Apium graveolens* (celery), *Origanum vulgare* (oregano), *Petroselinum crispum* (parsley)	[67]
	Luteolin	*Cucurbita* spp. (pumpkin), *Daucus carota* (carrot), *Capsicum* spp.	[68,69]
	Baicalein	*Scutellaria* spp. (skullcap), *Thymus vulgaris* (thyme)	[70]
	Chrysin	Honey, *Passiflora* spp. (passionflower)	[71]
	Acacetin	*Carthamus tinctorius* (safflower), *Chrysanthemum* spp. (Chrysanthemum), *Linaria* spp. (Linaria)	[72]
Flavonols	Galangin	Honey, *Alpinia* spp. (ginger)	[73]
	Quercetin	*Allium cepa* (red onion), *Malus domestica* (apple), *Vaccinium* spp. (cranberry)	[74–76]
	Kaempferol	*Anethum graveolens* (dill), *Spinacia oleracea* (spinach), *Brassica oleracea* (kale)	[76]
	Myricetin	*Lycium* spp. (goji), *Vaccinium* spp. (blueberry), *Ceratonia siliqua* (carob)	[77]
	Morin	*Psidium guajava* (guava), *Artocarpus heterophyllus* (jackfruit)	[78,79]
	Fisetin	*Prunus persica* (peach), *Fragaria* × *ananassa* (strawberry), *Diospyros* spp. (persimmon)	[80]
Flavanonols (Dihydroflavonols)	Taxifolin	*Camellia sinensis* (black tea), red wine, *Allium cepa* (onion)	[81,82]
	Ampelopsin	*Rhododendron* spp. (Rhododendron), *Nekemias grossedentata* (vine tea)	[83,84]
	Aromadendrin	*Hamamelis virginiana* (witch hazel), *Phoenix dactylifera* (dates), *Lentinula edodes* (shiitake mushrooms)	[85]
	Astilbin	*Vitis vinifera* (grape), *Hypericum perforatum* (St John's wort)	[86]
Flavanols (Flavan-3-ols)	Catechin	Red wine, *Malus domestica* (apple), *Pyrus* spp. (pear)	[87]
	Epicatechin	*Camellia sinensis* (green tea), *Malus domestica* (apple), *Theobroma cacao* (cocoa)	[88]
	Epigallocatechin	*Persea americana* (avocado), *Pistacia vera* (pistachio), *Actinidia chinensis* (kiwifruit)	[87,89]
	Gallocatechin	*Camellia sinensis* (green tea), *Prunus armeniaca* (apricots), *Rubus fruticosus* L. *agg.* (blackberries)	[90–92]
Isoflavones	Genistein	*Cicer arietinum* (chickpea), fermented soybeans (tempeh), *Vicia faba* (fava bean)	[93,94]
	Daidzein	*Pueraria montana* (kudzu root), *Glycine max* (soybean), tofu	[95,96]
	Formononetin	*Trifolium pratense* (red clover), *Glycyrrhiza* spp. (licorice), *Astragalus* spp.	[97–99]
	Glycitein	*Glycine max* (soybean), tofu	[100]
	Biochanin A	*Trifolium pratense* (red clover), *Glycine max* (soybean), *Arachis hypogaea* (peanut)	[101]

4.2.2. Summary of the Two Primary Flavonoid Assays

The $AlCl_3$-based colourimetric assay for Total Flavonoid Content (TFC) determination exists in two primary variations involving sodium nitrite ($NaNO_2$) addition and one alternative method without $NaNO_2$. The original protocol developed by Christ and Müller [102] relies on the direct complexation of $AlCl_3$ with flavonoids, forming a yellow-orange complex measurable at 415 nm. However, this method lacks specificity, as it does not differentiate flavonoid subclasses and is prone to interference from other polyphenolic compounds. Despite its simplicity, it is limited in its ability to quantify total flavonoids

accurately. To improve specificity, the work by Barnum [103] was applied to develop the $NaNO_2$-$AlCl_3$-NaOH assay, which follows a sequential reaction process. This method was largely popularised by the work of Zhishen, et al. [104] who used the $NaNO_2$-$AlCl_3$-NaOH assay to determine flavonoids content in mulberry fruits. In this method, $NaNO_2$ first reacts with flavonoids containing o-dihydroxy (catechol) groups, forming a diazonium salt intermediate. $AlCl_3$ is then added, facilitating complex formation, and finally, NaOH stabilises the colour change, allowing spectrophotometric measurement at 510 nm. This method is commonly used for flavonols, flavones, and flavanones, although it has limited applicability to other flavonoid subclasses. A variation of this, the $NaNO_2$-$AlCl_3$-KOH assay, follows a similar reaction mechanism, but KOH is used instead of NaOH in the final step. KOH is proposed to enhances solubility, making this method more effective for flavonoids in plant extracts and beverages [18].

Mechanistically, the $AlCl_3$-based assays operate through the chelation of flavonoid hydroxyl and keto groups by aluminium ions, which modifies their electronic conjugation and produces visible absorbance shifts. The sequence of reactions differs between the direct and $NaNO_2$-based methods, as outlined below:

Direct $AlCl_3$ Assay:

- Chelation: Al^{3+} coordinates with flavonoid functional groups, primarily:
  - C-4 keto + C-5 hydroxyl groups (C ring)
  - 3′,4′-dihydroxy (catechol) groups (B ring)
- Complex formation: Stable flavonoid–Al^{3+} complexes are produced.
- Colour development: Coordination alters conjugation within the flavonoid backbone, generating a yellow complex with absorbance at ~415 nm.

$NaNO_2$–$AlCl_3$–NaOH/KOH Assay:

- Diazotization: $NaNO_2$ reacts with o-dihydroxy (catechol) groups on the B ring, forming diazonium intermediates.
- Chelation: Al^{3+} binds to hydroxyl and keto groups, reinforcing complex stability.
- Stabilisation: NaOH or KOH deprotonates remaining hydroxyl groups, enhancing solubility and inducing bathochromic shifts.
- Colour development: The final complex exhibits an orange–red colour with absorbance at ~510 nm.

4.2.3. Coordination Mechanisms and Spectral Behaviour of Common Flavonoid Standards (Quercetin, Catechin, and Rutin) Used in $AlCl_3$-Based Assays

Among flavonoid assay calibration standards, quercetin, catechin, and rutin are the most widely employed in $AlCl_3$-based TFC assays due to their structural diversity, commercial availability, and representation of the three dominant subclasses (flavonols, flavan-3-ols, and flavonol glycosides) [105]. These compounds exhibit distinct chelation behaviours that influence colour development, spectral response, and analytical sensitivity [105]. Their differing metal-binding motifs and degrees of conjugation provide valuable insight into how structural variations govern chromophore formation and assay performance. Coordination typically involves hydroxyl and carbonyl sites capable of donating lone-pair electrons to the metal centre, thereby extending π-electron delocalisation through the chromone nucleus [18,105,106]. This redistribution of charge lowers the $\pi \rightarrow \pi^*$ transition energy and produces the bathochromic shift near 510 nm that defines Al^{3+}–flavonoid chromophores.

Flavonols such as quercetin exhibit the strongest colour development because their 5-hydroxyl and 4-carbonyl groups form a stable six-membered chelate with Al^{3+}, while the adjacent 3′,4′-dihydroxyl (catechol) moiety on the B ring can participate in secondary coordination (Figure 8). Under $NaNO_2$/NaOH conditions, partial oxidation of this catechol

site generates phenolate donors that further stabilise the complex and intensify absorbance (Figure 8). In contrast, flavan-3-ols such as catechin, which lack both the 4-carbonyl and the C2=C3 conjugation present in flavonols, chelate mainly through the catechol site on the B ring (Figure 8). The resulting five-membered complex is less conjugated and produces a weaker, more localised spectral response. Glycosylated flavonols such as rutin, where the 3-hydroxyl is substituted by a rutinoside group, lose the 3-OH/4-keto chelation site and experience steric restriction around the C ring. Therefore, aluminium coordination occurs primarily through the B-ring catechol, leading to reduced molar absorptivity compared with the aglycone (Figure 8).

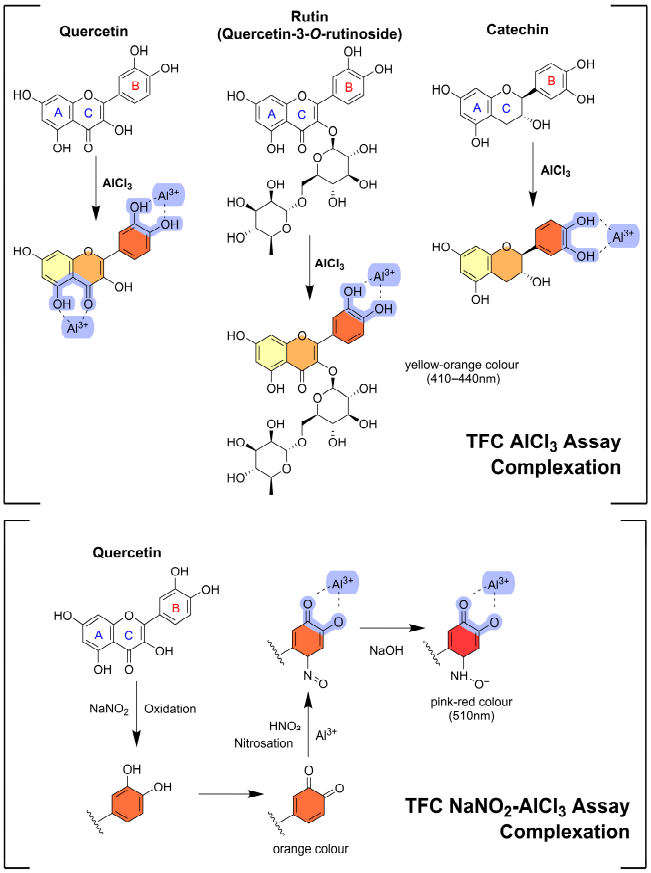


Figure 8. Simplified mechanisms underlying flavonoid complexation in the $AlCl_3$ TFC assay and the modified $NaNO_2$–$AlCl_3$ assay. (**Top**) In the standard $AlCl_3$ method, quercetin, rutin, and catechin form characteristic six/five-membered Al^{3+} chelate complexes primarily at the 3-OH/4-keto site (and secondarily at the 4-keto/5-OH site), producing the yellow–orange chromophore ($\lambda_{max} \approx 410$–$440$ nm). The extent of chelation is influenced by the availability of free hydroxyl groups and by glycosylation at C-3, as shown for rutin. (**Bottom**) In the $NaNO_2$–$AlCl_3$ variant, nitrosation of the electron-rich B-ring produces a transient nitroso intermediate that rearranges through a diazonium-like state to form an o-quinone, enhancing conjugation across the flavonoid skeleton. Subsequent Al^{3+} coordination at the 3-OH/4-keto site, followed by deprotonation with NaOH, yields a strongly conjugated Al^{3+}–flavonoid complex responsible for the characteristic pink–red chromophore ($\lambda \approx 510$ nm). Together, these pathways illustrate the structural basis for colour development in both TFC assay formats. Mechanistic steps shown are schematic representations intended to illustrate likely reaction pathways in TFC assay conditions; they are not drawn as full electron-pushing mechanisms.

4.2.4. Critical Evaluation of the $AlCl_3$ Assay

A critical evaluation by Shraim, et al. [18] highlighted several inconsistencies in accuracy and reliability of the TFC assay, which researchers often overlook. Spiked recovery

experiments, conducted with catechin, quercetin, and rutin, demonstrated significant variability in absorbance values, leading to unreliable flavonoid quantification across both $NaNO_2$-based and non-$NaNO_2$ methods [18]. When quercetin and rutin were interchanged as quantification standards, false-positive (63–124%) and false-negative (26–42%) results were observed, while unacceptable spike recoveries (8–106%) further highlighted the methods limitations. In plant extracts, TFC values fluctuated drastically (58–152%), depending on the chosen standard, while the addition of $NaNO_2$ resulted in over- or underestimation of flavonoid content [18].

Given these issues, proper standard selection is crucial, particularly when the flavonoid composition of an extract is known. For example:

- The $NaNO_2$-$AlCl_3$-NaOH assay is more specific for flavan-3-ols and should be used with catechin as the standard [18].
- The $AlCl_3$-NaOH assay requires quercetin as the most reliable standard for flavonol and flavone rich samples [18].

More recently, Nicolescu, et al. [107] conducted an extensive comparative evaluation of colourimetric assays for TFC determination. Their findings reaffirmed that while the $AlCl_3$ assay remains widely used due to its simplicity and cost-effectiveness, it suffers from poor specificity and interference from non-flavonoid compounds, further compromising accuracy. Through methodological comparison, Nicolescu, et al. [107] identified the lesser-used sodium borohydride–chloranil (SBC) assay by He, et al. [108] as the only method capable of accurate total flavonoid quantification. The review by Nicolescu, et al. [107] strongly advocates for restructuring laboratory protocols to incorporate more reliable assays like SBC for plant and food analysis, reinforcing its superiority over conventional $AlCl_3$-based methods. However, despite its accuracy, SBC is not commonly used due to its extensive protocol and lower throughput compared to $AlCl_3$-based methods. Despite these large inaccuracies of the TFC assay that have been outlined, the $AlCl_3$ assay remains in widespread use because its results often correlate positively with TPC and antioxidant activity when analysed using Pearson's correlation coefficient [109].

4.2.5. Alternative Approaches to TFC Determination and Best Practice

Given the challenges associated with flavonoid content determination, researchers should adopt a structured approach to ensure accuracy and reproducibility. However, in some instances simplified flavonoid assays may also prevail as reliable routine assays. For example, direct UV–Vis spectrum analysis can be used when the flavonoid profile of a sample is chemically simple or dominated by a single subclass, such as flavonols. In the method by Rolim, et al. [110] no complexing reagents are required, instead, quantification is achieved by recording the native UV–Vis absorption spectrum of the extract and comparing the absorbance at a characteristic wavelength (typically around 360–370 nm for flavonols like rutin) with that of a calibration curve constructed from a flavonoid standard. Because the method by Rolim, et al. [110] relies on inherent spectral features rather than secondary colour formation, it is most appropriate for standardised extracts with minimal matrix interference and when flavonoid subclasses exhibit distinct absorbance maxima. The following stepwise guide outlines best practice approach in light of the above discussions in this chapter:

Step 1: Identify the Dominant Flavonoid Class

- Determine the major flavonoid class in the sample using liquid chromatography (LC) [111].
- If LC analysis is unavailable, conduct a literature review to assess whether flavonols, flavanones, flavan-3-ols, or anthocyanins are likely dominant in the sample.

Step 2: Select the Most Suitable Assay

- Choose a validated method that aligns with the flavonoid class present to improve assay specificity and prevent underestimation or overestimation [107].
- Recommended method: The SBC assay is a reliable choice for comprehensive flavonoid determination [108], but it is not high-throughput.

Step 3: Use Matrix-Specific Methods When Necessary

- If flavonoid profiling is not feasible and SBC is unsuitable, select an assay that best aligns with the sample matrix.
- Example: The optimised TFC assay for honey serves as a guide for method adaptation in specific matrices [106]. In addition, optimised methods for citrus flavonoids have been identified using multiple standards and reaction conditions [112].

Step 4: Adopt Multiple Complementary Assays

- No single method can reliably quantify total flavonoids; therefore, multiple complementary assays should be used.
- Best practice: Pair the $AlCl_3$ assay with subclass-specific methods.
    - DNPH for flavanones (e.g., bee products) [113].
    - DEG-NaOH for flavanone-rich fruits [112,114].
    - DMACA for catechins and proanthocyanidins [115].
    - SBC for comprehensive flavonoid quantification [108].

4.2.6. Comparison of Benchmark Parameters for TFC Determination Using ACl_3 and UV–Vis Methods

The comparative benchmark data presented in Table 3 summarise the analytical characteristics and performance of commonly applied TFC determination methods using $AlCl_3$ and ultraviolet–visible UV–Vis spectrophotometry. The classical $NaNO_2$–$AlCl_3$–NaOH method remains the most validated, combining nitrosation, Al^{3+} chelation, and alkaline stabilisation steps to yield a pink-red complex with a characteristic absorbance maximum at approximately 510 nm [44]. In contrast, $AlCl_3$-based variants employing direct complexation (410–440 nm) or modified reagent sequences exhibit greater variability and standard-dependent bias, limiting cross-method comparability.

Alternative direct UV–Vis approaches forego derivatisation chemistry, instead quantifying native flavonoid chromophores through characteristic UV absorption bands (notably $\approx$ 361 nm). The introduction of high-throughput microplate adaptations of the $NaNO_2$–$AlCl_3$–NaOH protocol has further enhanced analytical efficiency, demonstrating strong correlation with cuvette-based measurements while significantly lowering reagent volumes and increasing sample throughput.

As shown in Table 3, validated $AlCl_3$ assays generally achieve high linearity ($r^2 \geq 0.995$) and precision (CV $\leq$ 10%) with recoveries exceeding 87%, whereas unstandardised variants reported in the literature may produce recoveries spanning several folds depending on wavelength and calibration choice. The microplate format offers a substantial gain in efficiency, enabling up to 60–90 samples per day, with only minor procedural differences from the conventional format. Collectively, these data highlight that while $AlCl_3$-based complexation remains the reference method for broad TFC quantification, direct UV–Vis analysis may serve as a complementary approach for routine screening when compositional simplicity permits.

Table 3. Comparative benchmark parameters for TFC determination using $AlCl_3$ and UV–Vis methods.

Method	$NaNO_2$–$AlCl_3$–NaOH	$AlCl_3$ Variants (Direct ± Acetate; $NaNO_2$/NaNO3–$AlCl_3$–NaOH)	Direct UV Method	Microplate High-Throughput $NaNO_2$–$AlCl_3$–NaOH
Reference	[116]	[18]	[110]	[117]
Cuvette/Microplate	Cuvette	Cuvette	Cuvette	Microplate (96-well)/ Cuvette reference
Principle	Nitrosation ($NaNO_2$) → Al^{3+} chelation → NaOH stabilisation → pink–red complex.	Al^{3+} chelation (yellow-orange 410–440 nm) or $NaNO_2$ route (≈510 nm); major λ/standard-dependent bias.	Direct absorbance of rutin-like UV banding (no derivatisation).	Nitrosation ($NaNO_2$) → Al^{3+} chelation → NaOH stabilisation → orange–red complex.
λ_{max} (nm)	510	410–440 (direct); ≈510 (with $NaNO_2$).	UV–Vis spectrum 200–400 nm: 361 (primary), 258 (secondary).	510/510
General protocol	800 µL H_2O + 200 µL sample; 60 µL $NaNO_2$ (5% *w*/*v*, 5 min) → 60 µL $AlCl_3$ (10%, 6 min) → 400 µL NaOH (1 M) + 480 µL H_2O	2.0 mL methanol + 0.5 mL sample; 0.20 mL AlCl3 (10% *w*/*v*), mix and 3 min at 25 °C → 0.20 mL CH_3COONa (1.80 g/mL, when used), and the final volume was made to 5.0 mL using methanol. When $NaNO_2$ was used: 2.0 mL + 0.5 mL sample → 0.15 mL $NaNO_2$ (1.0 mol/L), mix and 3 min at 25 °C → 0.15 mL $AlCl_3$ (10% *w*/*v*), mix and 3 min at 25 °C → 1 mL NaOH (1 mol/L), and the final volume was made to 5.0 mL using methanol. Final solutions mixed stored in dark for 40 min at 25 °C.	Plant extract *T. catigua* Adr. Juss and *P. olacoides* Bentham commercial	800 µL H_2O + 200 µL sample; 60 µL $NaNO_2$ (5% *w*/*v*, 5 min) → 60 µL $AlCl_3$ (10%, 6 min) → 400 µL NaOH (1 M) + 480 µL H_2O
Linear range	All standards were prepared in mg L^{-1}: Catechin 1–200; Procyanidin B1 1–100; Procyanidin B2 1–300; Quercetin 1–500; Rutin 1–500; Phloretin 1–1000; Phloretin-2-glc 1–1000.	1–70 µg mL^{-1} at six wavelengths (400, 410, 415, 420, 430, and 440 nm)	5–15 µg mL^{-1} rutin.	5–250 µg mL^{-1} catechin (microplate)/5–250 µg mL^{-1} catechin (cuvette).
r^2 (linearity)	≥0.995 across standards.	AlCl3 method: Quercetin–0.999; Rutin–0.998/$NaNO_2$–$AlCl_3$ method: Quercetin > 0.991; Catechin > 0.998. All measured at various wavelengths.	0.9997. Slope = 0.0293	0.9983 (y = 0.0022x + 0.019)/0.9996.
LOD/LOQ	Catechin 0.88/2.65 mg L^{-1}; Quercetin 0.42/1.29 mg L^{-1}; Procyanidin B1 1.65/5.00 mg L^{-1}; Procyanidin B2 0.33/1.01 mg L^{-1}; Quercetin-3-rutinoside 0.90/2.72 mg L^{-1}; Phloretin 2.33/7.07 mg L^{-1}; Phloretin-2-glucoside 2.33/7.07 mg L^{-1}	Not evaluated; shows large recovery bias instead.	0.09/0.27 µg mL^{-1}.	Not stated (microplate method validated via recovery/precision).
Precision	Intra 0–12.2% CV; inter 0–9.5% CV.	Qualitative; no numeric precision, but large bias vs. standard/λ.	Intra 0.30–0.49%, inter 0.31–0.81%.	Microplate; inter: 127.90 ± 1.70 (CV %: 1.33) intra: 126.69 ± 2.65 (CV %: 2.09).
Accuracy/recovery	87–115%.	Spike recoveries can span 33–343% depending on standard/λ.	99.36–102.14% recovery. Accuracy: Intra 100.67–102.38%, inter 98.58–100.38%.	Microplate; Recovery: 102.65–103.40%. CV: 1.06–2.15%.
Selectivity notes	Best for catechol-bearing flavan-3-ols & flavonols; weaker for dihydrochalcones.	Acetate offers no benefit; $NaNO_3$ does not improve suitability.	Extract vs. rutin spectra identical at 361 nm (specificity proof).	Microplate reproduces cuvette λ and response; strong agreement (r = 0.993).
Preferred standard	Catechin/Procyanidin B2 (flavan-3-ols); Quercetin/Rutin (flavonols).	Must match subclass; results are standard-dependent.	Rutin.	Catechin/Catechin
Expression	mg Catechin or Quercetin or Rutin per g $^{-1}$	mg Catechin or Quercetin or Rutin per g $^{-1}$	mg Rutin Eq g^{-1} extract.	mg CE g^{-1} (both).
Throughput/reagents	Single-sample workflow; large volumes (~5–10 min pipetting per sample)	Single-sample workflow; 15 min of pipetting and long incubation time in the dark	Low-throughput manual spectra.	Up to 64 samples day^{-1}; ~225 µL reagents per well/20–24 samples day^{-1}; ~5.8 mL per sample.
Best use case	Flavan-3-ol-rich extracts (tea, grape, cocoa).	Method bias evaluation; choose variant only with subclass clarity.	Rutin-dominant extracts for QC.	High-throughput microplate screening with strong concordance to cuvette.

Data summarise representative benchmark studies of Total Flavonoid Content (TFC) assays using aluminium chloride ($AlCl_3$) and direct UV–Vis spectrophotometric approaches. Reported values correspond to the cited conditions without re-normalisation. Abbreviations: CE, catechin equivalent; CV, coefficient of variation; LOD, limit of detection; LOQ, limit of quantification; λ_{max}, wavelength of maximum absorbance. Differences in solvent system, reaction time, and reference standard contribute to inter-method bias. → symbol indicates the sequential step in the assay method.

4.3. Anthocyanins

Anthocyanins belong to the flavonoid family and share the common flavone backbone of flavonoids (Figure 6). They are distinguished by the presence of a positively charged, glycosylated flavylium cation, which contributes to their pigmentation and characteristic pH-dependent colour variation [25]. These compounds are widely distributed in nature and are responsible for the red, purple, and blue pigmentation in many fruits, vegetables, and flowers. Due to their potential antioxidant, anti-inflammatory, and neuroprotective effects, anthocyanins are of considerable interest in nutraceutical and functional food research [25].

4.3.1. The pH-Differential Method for TMAC Quantification

The original pH-differential method used to determine Total Monomeric Anthocyanin Content (TMAC) was proposed by Sondheimer and Kertesz [118] and involved measuring UV absorbance at two distinct pH values to quantify the anthocyanins of strawberries. Over time, several modifications of this technique have been introduced in the scientific literature. A notable study by Rapisarda, et al. [119] evaluated five different spectrophotometric methods and identified a reliable approach for analysing fruit juices. Their method utilised buffer solutions and measured absorbance at 510 nm, expressing results as cyanidin-3-glucoside (C3G) chloride equivalents. The work by Rapisarda, et al. [119] laid the foundation for the pH-differential method, which was standardised by Lee, et al. [33] and adopted as AOAC 2005.02. The method by Lee, et al. [33] provides a simple, rapid, and cost-effective alternative for high-throughput anthocyanin quantification. Its applicability was further validated in a study comparing a microplate reader adaption with HPLC-based quantification [120]. From a total of 517 replicate analyses, Lee, et al. [120] reported a strong correlation coefficient (R^2 = 0.931) between the pH differential method and HPLC for various berry and wine samples, underscoring its reliability for anthocyanin research. The AOAC-TMAC method operates on the principle that anthocyanins undergo pH-dependent structural transformations, allowing for quantification based on their spectral changes where:

- At pH 1.0, anthocyanins exist in their coloured oxonium form.
- At pH 4.5, they predominantly convert to a colourless hemiketal form.

Figure 9 displays the pH dependent spectral behaviour of anthocyanins using UV–Vis data from crude *Antidesma erostre* extracts (Australian native currants) [121]. At pH 1.0, the flavylium cation is stabilised, giving rise to a strong absorption band in the visible region. When the pH is increased to 4.5, hydration to the colourless hemiketal suppresses the visible absorbance. The arrow in Figure 9 highlights both the decrease in absorbance and the slight bathochromic shift of the λ_{max}, which commonly occurs as the chromophore relaxes toward a less conjugated and hydrated form. This spectral contrast forms the basis of the pH-differential method, where the difference in absorbance between pH 1.0 and pH 4.5 (ΔA) is directly proportional to the TMAC. Correction at 700 nm remains essential for removing background scattering from crude extracts. For reliable quantification, spectra should be recorded at appropriate dilutions to ensure absorbance values fall within the linear range of approximately 0.1–1.0 AU.

The difference in absorbance maxima between these two pH conditions is directly proportional to the TMAC [33,119,120,122]. Additionally, absorbance at 700 nm is measured to correct for light scattering, turbidity, and background interference [122], and this step must not be overlooked as Figure 9 clearly demonstrates a change in absorbance at 700 nm

between pH 1.0 and 4.5. According to AOAC 2005.02, the anthocyanin concentration is calculated using Equation (5):

$$Total\ Anthocyanins\ \left(\frac{\text{mg}}{\text{L}}\right) = \frac{A \times MW \times DF \times 10^3}{\varepsilon \times l} \quad (5)$$

where

- $A = (A_{max} - A_{700\text{nm}})\ \text{pH}_{1.0} - (A_{max} - A_{700\text{nm}})\ \text{pH}_{4.5}$
- MW = Molecular Weight of cyanidin-3-glucoside (449.2 g/mol).
- DF = Dilution Factor
- 10^3 = Conversion factor (g to mg).
- ε = molar extinction coefficient of cyanidin-3-glucoside (26,900 $\text{L}\cdot\text{mol}^{-1}\cdot\text{cm}^{-1}$)
- l = Path length of the cuvette (usually 1 cm).

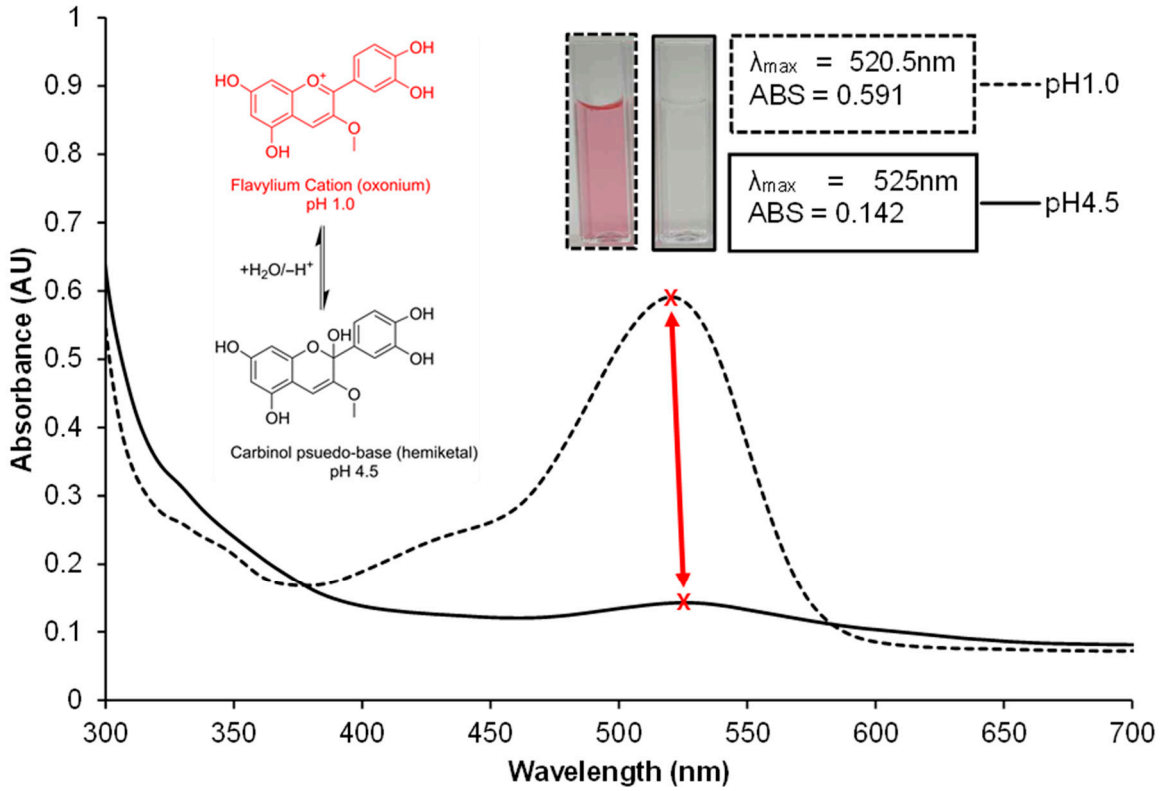


Figure 9. UV–Vis spectra of *Antidesma erostre* (Australian native currants) at pH 1.0 and pH 4.5 showing the pH-dependent structural transition of their anthocyanins. At pH 1.0, anthocyanins exist primarily as flavylium cations with a strong visible absorption band; at pH 4.5, modification to the colourless hemiketal greatly reduces absorbance. The arrows indicates the absorbance difference and the bathochromic shift in λ_{max} accompanying pH-induced structural change. "X" marks the λ_{max} for each spectrum.

4.3.2. Accurate Application of the TMAC Assay

While the pH-differential method is widely employed in quality assurance workflows within the wine, pigment, and fruit juice industries due to its simplicity, speed, and reproducibility, its application in crude plant extract analysis for nutraceutical research often lacks the necessary scrutiny. A major issue arises from its widespread use without considering anthocyanin distribution and sample purity. Similar to the TFC assay, the pH-differential method is frequently applied without fully accounting for the structural variability of anthocyanins populations across different plant matrices [123]. Improper application of the AOAC 2005.02 method assumes that C3G is the predominant anthocyanin

present, and all results are expressed as C3G equivalents per litre or per gram of sample. While this assumption holds true for certain food sources, it is not universally applicable, leading to potential inaccuracies when dealing with anthocyanin-rich matrices containing a more diverse composition of anthocyanins [123].

The original work by Lee, et al. [33] recognises this limitation, yet the method has often been adopted without careful consideration of the molar extinction coefficients (ε) required for accurate quantification. The six major anthocyanin families, pelargonidin, cyanidin, delphinidin, peonidin, petunidin, and malvidin (Figure 10), differ in their hydroxylation and methylation patterns, which influence both colour and stability [124]. Increased hydroxylation, as seen in delphinidin, tends to shift the colour spectrum from red to blue, whereas increased methylation, as in malvidin, stabilises the molecule and results in a more purplish hue [125]. These structural differences influence their absorbance maxima (λ_{max}) within the visible spectrum (400–700 nm) and, importantly, their molar absorptivity values [126]. Since the pH-differential method relies on measuring absorbance at a fixed 520 nm when expressing results in C3G equivalents, significant errors can occur if the predominant anthocyanins in the sample have λ_{max} values that deviate from this wavelength.

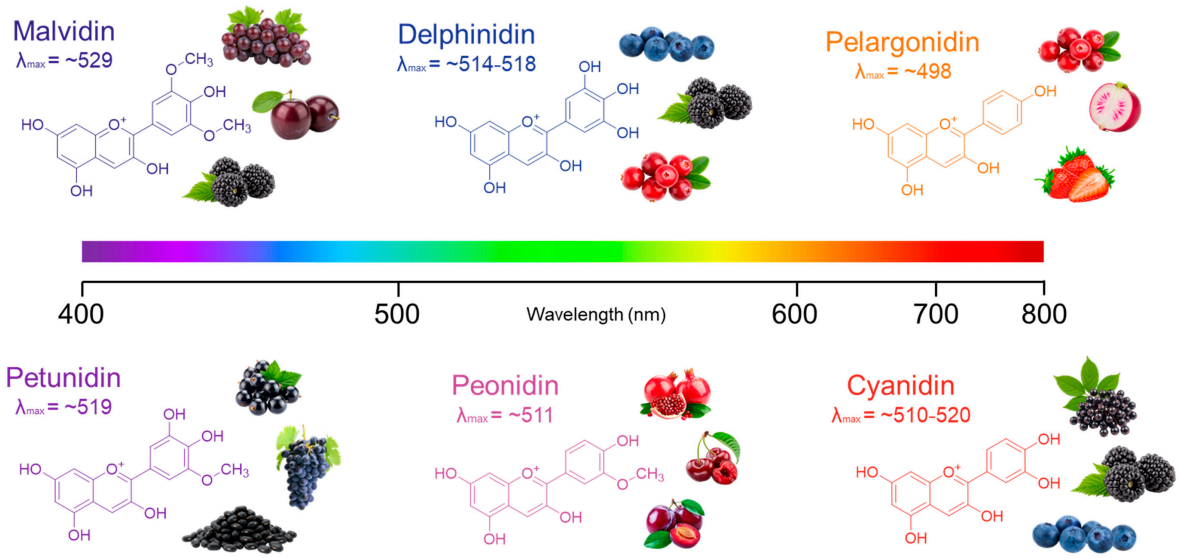


Figure 10. Representative anthocyanidin structures, their approximate λ_{max}, and corresponding fruit sources commonly found in nature. Each anthocyanidin differs by the number and position of hydroxyl (–OH) and methoxy (–OCH_3) substituents on the B-ring, which directly influence hue and spectral properties. Pelargonidin ($\lambda_{max} \approx 498$ nm) contributes to orange–red pigmentation; cyanidin ($\lambda_{max} \approx 510$–520 nm) to red–purple; peonidin ($\lambda_{max} \approx 511$ nm) to pink–magenta; petunidin ($\lambda_{max} \approx 519$ nm) to bluish-purple; delphinidin ($\lambda_{max} \approx 514$–518 nm) to blue–violet; and malvidin ($\lambda_{max} \approx 529$ nm) to deep purple–blue tones. The spectral gradient (centre) illustrates the progressive bathochromic shift in λ_{max} associated with increasing hydroxylation or methoxylation on the B-ring. Malvidin: *Prunus domestica* (Black Plum), *Vitis vinifera* (Red Grape), *Rubus subg. rubus* (Blackberry). Delphinidin: *Rubus* subg. *rubus* (Blackberry), *Vaccinium* spp. (Blueberry), *Vaccinium* subg. *Oxycoccus* (Cranberry). Pelargonidin: *Vaccinium* subg. *Oxycoccus* (Cranberry), *Raphanus sativus* var. *sativus* (Red Radish), *Fragaria x ananassa* (Strawberry). Petunidin: *Ribes nigrum* (Blackcurrant), *Vitis vinifera* (Black Grape), *Phaseolus vulgaris* (Black Bean). Peonidin: *Punica granatum* (Pomegranate), *Prunus avium* (Cherry), *Prunus domestica* (Red Plum). Cyanidin: *Sambucus* spp. (Elderberry), *Rubus* subg. *rubus* (Blackberry), *Vaccinium* spp. (Blueberry).

Beyond the structural differences among anthocyanins, molar absorptivity values are highly dependent on the analytical conditions used. Several studies have demonstrated that ε values fluctuate based on the purity of analytical standards, solvent composition, and the

type of acid used for pH adjustment [126,127]. Singh, et al. [128] highlighted this variability in a study evaluating anthocyanin content in Australian blueberries. They compared four approaches: LC-MS quantification of individual anthocyanins, the pH-differential method expressed as C3G equivalents at 520 nm, the pH-differential method expressed as malvidin-3-glucoside (M3G) equivalents at 520 nm, and the pH-differential method expressed as M3G equivalents at λ_{max} (521 nm). Their findings revealed that the standard pH-differential method, which relies solely on C3G ε values (21.24 mg), underestimated anthocyanin content by 119.9% when compared to LC-MS data. However, when the molar absorptivity of M3G was applied in place of C3G, the anthocyanin content (102.91 mg and 103.22 mg M3G equivalent for 520 nm and λ_{max}: 521 nm respectively), aligned closely with the LC-MS measured value (84.88 mg/100 g FW).

These findings underscore the need for careful application of the pH-differential method, particularly when analysing diverse food and plant matrices and correlating these values with nutraceutical potential [129]. While these steps form the foundation for understanding the scientific basis of any method [130], the improper application of the pH-differential method remains widespread. Numerous studies continue to express anthocyanin content in various food and plant extracts as C3G equivalents, even when cyanidin derivatives are not the predominant anthocyanin group. For example, Gündüz, et al. [131] analysed the TMAC of different blueberry cultivars across multiple seasons and expressed the data as C3G equivalents, despite the dominating anthocyanin being M3G. Likewise, Ali, et al. [132] investigated the anthocyanin content of various Australian native fruits and reported the TMAC content of muntries, quandong, and Davidson plum as C3G equivalents, while also reporting high resolution mass spectrometry data of individual anthocyanins demonstrating that the predominant species were indeed delphinidin derivatives. The assumption that C3G is the most abundant anthocyanin introduces systematic error when applied indiscriminately. However, this issue arises not from a limitation of the AOAC 2005.02 method itself but from its misapplication in research. Before employing the pH-differential method, researchers must first determine the predominant anthocyanin composition in their samples to assess whether C3G is an appropriate reference anthocyanin. If other anthocyanins, such as peonidin-3-glucoside or delphinidin-3-glucoside, are more prevalent, adjustments must be made by substituting the relevant ε values to improve quantification accuracy. Additionally, the absorbance maxima used in the Equation (5) must be adjusted accordingly.

The structural diversity among anthocyanins gives rise to distinct colouration patterns that correspond to specific absorbance maxima within the visible spectrum. Figure 10 illustrates the six major anthocyanidin aglycones commonly found in nutraceutical-rich fruits, highlighting how progressive hydroxylation and methylation on the B-ring influence both hue and λ_{max}. The visual spectrum demonstrates the bathochromic shift from orange–red pelargonidin (≈498 nm) through to the deep blue–purple malvidin (≈529 nm), reflecting the direct relationship between molecular substitution, colour intensity, and optical stability.

4.3.3. Reference Values for Anthocyanidin-3-O-glucosides Used for TMAC Quantification

Accurate TMAC estimation depends on the correct application of the ε and λ_{max} of the dominant anthocyanin present in the sample as described earlier in this chapter. Historically, Cabrita, et al. [133] provided the first systematic evaluation of the visible absorption maxima and ε values for purified anthocyanidin-3-O-glucosides in 0.02 M KCl buffer (pH 1.0). Their work established a pH-dependent framework for interpreting spectral behaviour and revealed consistent bathochromic shifts among hydroxylated versus methylated anthocyanidins. More recently, Singh, et al. [128] re-determined these

optical constants under identical solvent and buffer conditions using purified flavylium chloride salts and high-precision spectrophotometry. Their results confirmed Cabrita's general trends but reported slightly refined ε values, particularly for pelargonidin-3-glucoside and C3G, attributable to improved standard purity, spectral resolution, and calibration traceability.

Together, these two datasets define the modern benchmark range for anthocyanin absorptivity constants applicable to AOAC 2005.02 and related pH-differential methods. Cabrita, et al. [133] data remains invaluable for historical comparison and demonstrating solvent- and pH-dependent behaviour, while Singh, et al. [128] work provides the most reliable ε values for direct analytical use. Table 4 integrates both sources, reporting the cation-corrected molecular weight (for direct use in Equation (5)) and the corresponding chloride-salt mass, thereby enabling researchers to convert standard masses appropriately and substitute compound-specific ε values when the predominant anthocyanidin differs from C3G.

Table 4. Spectral and molar-absorptivity reference values for anthocyanidin-3-*O*-glucosides in 0.025 M KCl buffer (pH 1.0, 25 °C).

Anthocyanidin-3-O-glucoside	MW (Cation)	MW (Chloride Salt)	λ_{max} (nm)	ε (L mol^{-1} cm^{-1})	Apparent Hue (pH 1.0)	Reference
Pelargonidin-3-glu	433.4	468.8	498	14,300	Orange-red	[133]
			498	13,317	Orange-red	[128]
Cyanidin-3-glu	449.2	484.8	510	20,000	Bright red	[133]
			520	26,900	Crimson-red	[122]
			511	22,791	Crimson-red	[128]
Peonidin-3-glu	463.2	498.9	510	15,100	Red-purple	[133]
			511	14,131	Red-purple	[128]
Delphinidin-3-glu	465.2	500.8	514	13,000	Violet	[133]
			518	6969	Violet-blue	[128]
Petunidin-3-glu	479.2	514.9	515	21,300	Purple-violet	[133]
			519	11,198	Purple-violet	[128]
Malvidin-3-glu	493.4	528.9	517	23,400	Purple-blue	[133]
			521	6538	Purple-blue	[128]

All spectra were recorded in 0.025 M KCl buffer at pH 1.0 ± 0.05 and 25 °C. Colour designations correspond to visual appearance at this pH, where anthocyanins exist predominantly as flavylium cations. Minor ε discrepancies among sources reflect differences in standard purity and instrumental calibration, not changes in chromophore behaviour.

4.3.4. Best Practices for Accurate TMAC Quantification

The evidence supporting the need for adjustments is clear. To improve the accuracy and application of the AOAC 2005.02 pH differential method, researchers should adhere to the following stepwise guide:

Step 1. Identify the Major Anthocyanins in the Sample

- Before applying the pH differential method, determine the dominant anthocyanin composition using chromatographic and spectroscopic methods or via literature searching.
- This ensures that the correct molar absorptivity (ε) values are applied.

Step 2. Use Accurate Molar Absorptivity (ε) Values

- The ε values for different anthocyanins have been reported in the literature, however, Table 4 provides a sufficient summary of past and present values for quick reference and use in Equation (5).
- Applying the correct ε value for the dominant anthocyanin in the sample is essential for accurate TMAC quantification.

Step 3. Consider the Appropriate Wavelength (λ_{max})

- Anthocyanins exhibit λ_{max} shifts based on structure and solvent conditions.
- Measuring absorbance at the specific λ_{max} for the predominant anthocyanin rather than the default 520 nm improves accuracy.
- As displayed in Figure 9 the λ_{max} of the same sample at different pH experiences slight bathochromic shifts, necessitating the use of unique λ_{max} wavelength for pH 1.0 and 4.5.

Step 4. Modify the Standard Method When Necessary

- If the sample contains non-C3G-dominant anthocyanins, adjusting the ε value and/or wavelength is recommended.

4.3.5. Benchmark Parameters for TMAC Quantification Using AOAC 2005.02 and Its Microplate Comparison

Having established the theoretical basis and critical parameters governing accurate TMAC quantification, it is equally important to examine the validated analytical performance of the pH differential assay as recognised by the AOAC. Benchmark data provides context for the method's precision, reproducibility, and linear response under controlled conditions, serving as a reference point for laboratories adapting or miniaturising the protocol. Microplate adaptations have demonstrated near-identical analytical behaviour while offering substantial gains in efficiency and reagent economy. Table 5 summarises the validated parameters of both the conventional cuvette and 96-well microplate formats, illustrating their comparable accuracy and precision, strong correlation with HPLC quantification, and suitability for high-throughput pigment analysis across diverse matrices.

Table 5. Validated parameters for the pH-Differential Assay of Total Monomeric Anthocyanins (TMAC).

Parameter	TMAC Quantification Using AOAC 2005.02 and Its Microplate Comparison
Reference	[33,120,122]
Principle	Measures monomeric anthocyanins via colour change between pH 1.0 (flavylium cation, red) and pH 4.5 (hemiketal, colourless). $\Delta A = (A_{520-700})_{pH1} - (A_{520} - A_{700})_{pH4.5}$.
Buffers (pH)	0.025 M KCl (pH 1.0 ± 0.05) and 0.4 M sodium acetate (pH 4.5 ± 0.05). Use identical buffers for cuvette and microplate.
Wavelengths (λ_{max}/correction)	Primary 520 nm; 700 nm for haze correction. Instrument bandwidth ≤ 5 nm.
Reference standard/ε/MW	Cyanidin-3-glucoside (C3G) (MW = 449.2 g mol^{-1}; ε = 26,900 L mol^{-1} cm^{-1} at 520 nm). Malvidin-3-glucoside (M3G) $\varepsilon \approx$ 28,000 L mol^{-1} cm^{-1} for wine matrices.
Path length	Cuvette: 1 cm quartz cell. Microplate: ~0.56 cm optical path
Validated range	20–3000 mg L^{-1} (C3G eq); absorbance range 0.2–1.4 AU (linear Beer–Lambert response).
Precision (RSDr/RSDR)	AOAC collaborative study: RSDr 1.06–4.16%; RSDR 2.69–10.12%. Microplate CV < 5%, SD ≈ 0.04 mg C3G eq/100 mL.
Accuracy/Recovery Correlation with cuvette/HPLC	AOAC spike tests 95–105%. Microplate values within 5% of cuvette ($p > 0.05$). Microplate vs. cuvette r^2 = 0.985, slope ≈ 1.02; Microplate vs. HPLC r^2 = 0.925–0.931, $p \leq 0.05$ (n = 517).
Throughput	Cuvette ≈ 6 samples h^{-1}; microplate ≈ 10× higher (~60 samples h^{-1}) with ~200 µL per well (2–3 mL per cuvette). Reagent use down ~90%.
Advantages	High specificity for monomeric anthocyanins; validated across matrices; excellent cuvette–microplate agreement; low cost, high throughput.
Limitations/cautions	Excludes polymeric pigments and copigmented complexes; ε and λ_{max} must match dominant anthocyanidin; microplates require uniform filling and path-length correction.
Result expression	mg C3G eq L^{-1} (or mg C3G eq 100 mL^{-1}). Always state standard, ε, geometry (cuvette or plate), and calibration details.

This table summarises analytical performance parameters of the pH-differential assay for Total Monomeric Anthocyanins (TMAC) following AOAC Official Method 2005.02 and its 96-well microplate variant. Quantification is based on the absorbance difference between pH 1.0 (flavylium cation) and pH 4.5 (hemiketal form) at 520 nm–700 nm. Results are expressed as mg C3G equivalents L^{-1} (or 100 mL^{-1}) using ε = 26,900 L mol^{-1} cm^{-1}. Abbreviations: C3G, cyanidin-3-glucoside; M3G, malvidin-3-glucoside; ε, molar absorptivity; MW, molecular weight; RSDr, relative standard deviation of repeatability; RSDR, relative standard deviation of reproducibility; CV, coefficient of variation. Microplate data demonstrate strong linearity (R ≈ 0.98–1.02) and >90% reduction in reagent volume compared with cuvette format.

4.4. Tannins

Tannins are high–molecular-weight polyphenols classically divided into condensed tannins (proanthocyanidins; polymers of flavan-3-ols), hydrolysable tannins (gallo- and ellagitannins) [13,28], and phlorotannins (Figure 11). The ability of tannins to precipitate proteins, bind metal ions, and complex with polysaccharides underpins astringency, haze formation in beverages, and many purported nutraceutical effects [134,135]. From a nutraceutical perspective, tannins have attracted considerable attention due to their wide-ranging bioactivities, which include antioxidant, antimicrobial, anti-inflammatory, cardioprotective, and anticancer effects [14]. Condensed tannins, abundant in cocoa, grapes, and berries, have been associated with cardiovascular benefits through modulation of endothelial function and inhibition of lipid peroxidation [136], while hydrolysable tannins such as ellagitannins contribute to gut health via microbial conversion into bioactive urolithins [137]. Their protein-binding capacity also underlies potential antinutritional effects, reducing digestibility of dietary proteins and minerals if consumed in high amounts [13]. Meanwhile, there has been interest in the effect of phlorotannins on cardiovascular and diabetes related illnesses [138]. These characteristics highlight the importance of accurate tannin quantification, not only for food quality and sensory properties but also for understanding their therapeutic promise and limitations as nutraceutical candidates.

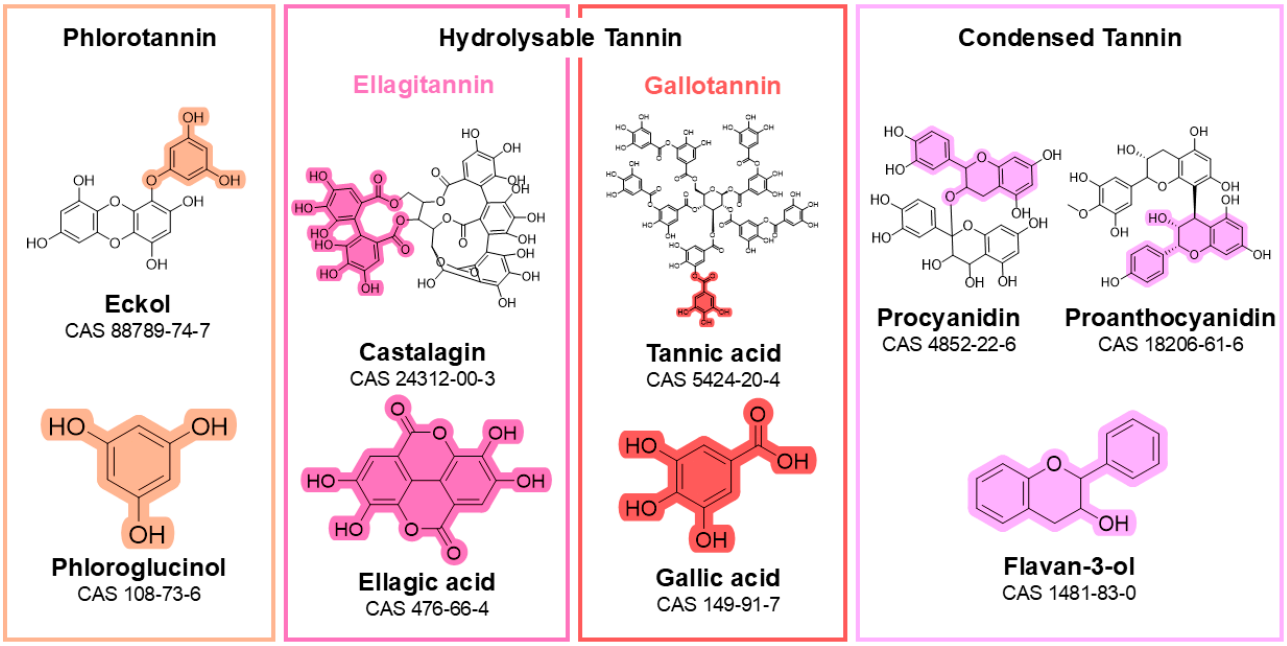


Figure 11. Representative tannin classes and their characteristic structural subunits. The major tannin categories phlorotannins, hydrolysable tannins (ellagitannins and gallotannins), and condensed tannins together with their key structural building blocks. Highlighted ring systems or core units (e.g., phloroglucinol for phlorotannins, hexahydroxydiphenoyl (HHDP) and galloyl groups for hydrolysable tannins, and flavan-3-ol subunits for condensed tannins) show the molecular features that define each tannin class.

In-vitro studies also demonstrate that tannin–protein binding is influenced by more than pH alone. While maximum precipitation often occurs near the isoelectric point of the protein, Perez-Maldonado, et al. [139] showed that condensed tannins can form insoluble complexes at higher, rumen-like pH values (6.0–6.5) in the presence of physiologically relevant inorganic ions (Ca^{2+}, Mg^{2+}, Na^{+}, K^{+}). This finding highlights that ionic strength and mineral composition can facilitate tannin–protein precipitation under conditions where pH alone would predict minimal interaction, emphasising the dynamic and environment-

dependent nature of tannin complexation in a nutraceutical context relating to human or animal consumption.

The quantification of tannins has a long history that reflects their importance in both industry and food science. The earliest assays in the 19th century relied on tannins' defining property of protein precipitation, with hide powder and gelatin gravimetry used to measure bark extracts for the leather industry [13]. One of the first chemical approaches was the Folin–Denis assay [140], which introduced a phosphotungstic–phosphomolybdic reagent to estimate "total tannins" and laid the groundwork for later phenolic assays described earlier. Modern advances emerged in the late 20th century, with the vanillin–HCl assay developed by Price, et al. [141] for flavan-3-ols and low–degree-of-polymerisation proanthocyanidins, and the butanol–HCl (Porter) assay by Porter, et al. [27], which provided a more reliable means of quantifying condensed tannins through acid depolymerisation to anthocyanidins. For hydrolysable tannins, colourimetric assays such as the rhodanine method were refined in the 1990s for gallotannin-rich foods [142]. These milestones collectively shaped the current suite of tannin assays, each with distinct advantages and limitations depending on the tannin class and sample matrix. For phlorotannins, the F–C assay remains the most widely used benchtop protocol, despite the limitations discussed earlier. Its dominance largely reflects its simplicity and adaptability, with many studies incorporating modifications such as hexane or dichloromethane defatting, antioxidant additions, or tailored solvent systems to minimise matrix interferences and improve extraction efficiency [29]. The DMBA assay is also used as a more selective alternative, targeting the 1,3- and 1,3,5-trihydroxybenzene moieties characteristic of phloroglucinol-based structures, although it can underestimate highly branched or substituted phlorotannins. Ford, et al. [29] provides a recent critical evaluation of these quantification methods, highlighting that even with these procedural adjustments, both assays have limitations in specificity and comparability, underscoring the need for more selective and standardised approaches for phlorotannin analysis.

Because tannins are chemically heterogeneous (subunit composition, interflavan linkages, degree of polymerisation, galloylation/hexahydroxydiphenoyl substitutions), no single colourimetric assay can accurately capture "total tannins" across food and plant matrices [13,27]. Consequently, authors who report "total tannin" values without acknowledging these structural complexities risk oversimplifying highly diverse polyphenol mixtures and generating data that are not directly comparable across studies or analytical methods. To address this challenge, a range of assays have been developed, each targeting specific tannin subclasses or functional properties. The following section critically evaluates the most widely applied methods, highlighting their strengths, limitations, and suitability for nutraceutical and food applications.

4.4.1. Vanillin-HCl Assay (For Flavan-3-ols/proanthocyanidins)

The vanillin–HCl assay is based on the condensation of vanillin with flavan-3-ol C-6/C-8 positions under acidic conditions, producing a red chromophore measurable at ~500–510 nm [143]. It is simple, inexpensive, and sensitive for monomers and low-DP oligomers [141]. However, it suffers from substantial limitations: (i) response varies with A-ring substitution and stereochemistry, underestimating polymer-rich samples [13,141]; (ii) sugars, anthocyanins, aldehydes, and ascorbate can enhance or suppress colour yield [141]; and (iii) results depend on the choice of standard, with catechin, epicatechin, or dimers giving markedly different values [27]. Therefore, the assay measures a reactive subset of flavan-3-ols rather than total tannins.

Detailed methodological work has shown that the vanillin–HCl assay is much more condition-sensitive than is often acknowledged. Sun, et al. [144] systematically evaluated "critical factors" for the vanillin reaction with both catechins and purified

oligomeric/polymeric proanthocyanidins (PA), demonstrating strong effects of acid type and normality, reaction time, temperature, water content, and reference standard at A_{500}. H_2SO_4 consistently gave higher sensitivity than HCl, but increasing acid strength also accelerated vanillin self-condensation and PA degradation, creating a trade-off between signal and artefact formation. Kinetics differed markedly between substrates: catechins reached a stable maximum within ~5–10 min, whereas PA showed slower, bell-shaped responses with subsequent decay, meaning that a fixed incubation time optimised on catechin standards can substantially misrepresent PA content. Even small amounts of water (≈3% v/v) reduced absorbance by ~50–60% for catechins and ~30–40% for PA, underscoring the need for essentially anhydrous methanolic media. Sun, et al. [64] also showed that expressing PA as "catechin equivalents" can either over- or underestimate true PA concentrations depending on acid strength. Only within a narrow H_2SO_4 range do catechin and oligomeric PA exhibit similar response factors, reinforcing the case for PA-based calibration standards and, where possible, chromatographic separation of catechins and PA prior to vanillin analysis.

In parallel, multivariate optimisation studies using design-of-experiments frameworks have confirmed that vanillin assays cannot be treated as plug-and-play methods. Khoshayand, et al. [145] applied a D-optimal response surface design to optimise five factors simultaneously and found that a full quadratic model explained >99% of the variance in absorbance, with acid strength and vanillin concentration exerting dominant effects. Optimal conditions derived in this way differed from widely adopted one-factor-at-a-time protocols and produced order-of-magnitude differences in signal for both catechin standards and fruit extracts. This work reinforces that vanillin-based assays cannot be treated as plug-and-play methods. Laboratories that simply copy published conditions without local optimisation and verification may obtain non-linear calibration curves, poor sensitivity, or systematically biased estimates when moving between standards and complex food matrices. Moreover, because the same chemistry can be tuned to sensitively detect both flavan-3-ols and anthocyanins, vanillin-based "total anthocyanin" or "total tannin" values are not directly comparable with results from structurally targeted methods such as pH-differential spectrophotometry or LC-based quantification.

4.4.2. Acid Butanol (Butanol-HCl, Porter) Assay

The butanol–HCl (Porter) assay relies on acid-catalysed oxidative depolymerisation of condensed tannins (proanthocyanidins) to anthocyanidins under heat, frequently with Fe^{3+} as catalyst, with absorbance typically measured around 550 nm [27,146,147]. This method is generally more effective than the vanillin assay for detecting higher polymer forms because it acts throughout the chain, but its conversion yield is dependent on monomeric subunit type, inter-flavan linkages, and modifications such as galloylation or methylation. Extreme assay conditions can also lead to degradation, side reactions, or interference from co-extracted sugars or pigments, thereby inflating absorbance readings. Moreover, the method underestimates bound condensed tannins, for example, Makkar, et al. [148] observed residual condensed tannin signals in ^{13}C NMR spectra of post-assay residues, indicating incomplete extraction or conversion. Because assay results are often expressed in "cyanidin equivalents", the assumed conversion factor rarely holds uniformly across different sample matrices, especially when polymer chain length and composition vary. Recent improvements that incorporate acetone in extraction and reagent systems have improved yield and linearity across soluble and insoluble proanthocyanidin fractions, but the core limitations due to structural heterogeneity and matrix interference remain [149].

Systematic and methodological studies on legumes highlight how sensitive the butanol–HCl assay is to extraction and reagent conditions. For example, Dalzell and Kerven [150] systematically optimised the assay for *Leucaena* spp. leaves and showed that

apparent PA content varied with water content, antioxidant type, Fe^{3+} concentration, and reagent: sample ratio. Back-extraction with diethyl ether and ethyl acetate led to partial loss of PA and selective removal of highly reactive fractions, systematically underestimating condensed tannins. In crude 70% acetone extracts, low PA samples could even show suppressed colour development while high PA samples were overestimated unless the matrix was re-optimised. By extracting with 70% aqueous acetone containing sodium metabisulphite, omitting Fe^{3+} from the butanol–HCl reagent, matching antioxidant concentrations between standards and samples, and using a 5:1 reagent: sample ratio, they achieved linear responses (25–1000 μg PA) and mean recoveries around 100%. These findings underscore that effective Porter-type assays depend not only on matrix-specific optimisation but also on step-dependent adjustments at each stage of extraction, sample preparation, and colour development. Treating the assay as a fixed, universally applicable protocol risks substantial under- or over-estimation of condensed tannins across different plant matrices.

Complementary work on extractable and bound PA in *Leucaena* spp. further shows that co-extractable pigments and other matrix components can substantially distort apparent "total-bound" PA if blank correction is not handled carefully [151]. Heated aqueous blanks (95% butanol/5% H_2O), which are widely used, underestimate the absorbance of co-extractable compounds and therefore overestimate bound PA, particularly in low-tannin tissues. In contrast, unheated acidic blanks (95% butanol/5% HCl) more accurately capture background absorbance for extractable PA, and wavelength-scanning approaches that fit a curved baseline to the full spectrum allow internal correction for each bound-PA sample matrix, recovering added anthocyanidins quantitatively. Therefore, effective Porter-type assays depend not only on matrix-specific optimisation, but also on step-dependent adjustments at each stage of extraction, blank correction, and colour development. Treating the assay as a fixed, universally applicable protocol risks substantial under- or over-estimation of both extractable and bound condensed tannins across different plant matrices.

4.4.3. DMACA (*p*-Dimethylaminocinnamaldehyde)

The DMACA assay involves electrophilic substitution at the flavan-3-ol C-6/C-8 positions under strongly acidic conditions, yielding a blue chromophore with absorbance maxima at ~640–670 nm [115]. It is highly selective for terminal catechin/epicatechin units, shows reduced interference from anthocyanins compared to the vanillin assay, and is widely used in seeds, cocoa, and teas. However, it has poor sensitivity for extension units and therefore systematically underestimates the contribution of highly polymerised proanthocyanidins [13,115]. Reported concentrations are typically expressed as catechin or epicatechin equivalents, but the lack of a universal extinction coefficient complicates cross-study comparisons. As it quantifies only terminal units, DMACA values are not directly comparable with those from butanol–HCl or vanillin assays. Matrix effects, particularly galloylation and the presence of other polyphenols, can further influence response factors. Beyond bulk quantification, DMACA is also used as a histochemical stain to visualise tannin distribution in plant tissues.

Evaluations of DMACA assay parameters highlight how strongly the chromogenic response depends on operational conditions [152]. Acid strength and identity, reagent concentration, reaction temperature, and even small amounts of residual water can materially alter colour yield, with water contents above ~1% causing significant bleaching at higher flavan-3-ol concentrations [152]. Reaction kinetics also vary by tannin size: monomers reach stable colour formation within 15 min, whereas oligomer-rich samples often require $\geq$20–35 min for complete development. These findings underscore that the apparent selectivity of DMACA for terminal units does not overcome its susceptibility to methodological variation. Protocols reported in the literature differ widely in acid normality, DMAC con-

centration, solvent purity, and timing, meaning DMACA values are rarely comparable across laboratories unless these parameters are explicitly controlled and reported. As such, the assay is best interpreted as a semi-quantitative index of terminal flavan-3-ols rather than a universal measure of "total proanthocyanidins".

4.4.4. Protein-Precipitation Assays

Protein-precipitation assays quantify tannins by measuring complexes with proteins such as BSA or gelatin [134,153] or with methylcellulose as a polymeric substitute [154]. These assays are functionally relevant, since they reflect the protein-binding behaviour underlying astringency, but they remain semi-quantitative rather than absolute measures of tannin content. Outcomes are highly dependent on assay conditions, including pH, ionic strength, ethanol concentration, and choice of protein, with different proteins showing selective affinities for tannins of varying size and hydrophobicity. While precipitation efficiency generally increases with degree of polymerisation, very large proanthocyanidins can remain soluble, and non-tannin phenolics may co-precipitate, compromising specificity [13]. Variants that pair precipitation with $FeCl_3$ colour development or HPLC analysis offer improved resolution, but comparability across studies remains limited. Reported values are usually expressed as catechin or tannic acid equivalents, yet the variable stoichiometry of protein–tannin interactions mean these equivalents are not chemically rigorous. Despite these limitations, protein-precipitation assays retain value for ranking samples and exploring functional relationships with astringency in foods and beverages.

Physiological studies also show that protein identity strongly alters precipitation behaviour. Perez-Maldonado, et al. [139] demonstrated that BSA exhibits relatively uniform binding capacity across tannin types, whereas plant leaf proteins (particularly Fraction 1/Rubisco) show distinct, tannin-specific responses that more closely reflect in-vivo dietary interactions. Importantly, salivary proteins did not form insoluble complexes under rumen-like conditions, instead forming predominantly soluble complexes, indicating that common BSA- or gelatin-based in vitro assays may not accurately represent protein interactions occurring during mastication or in the rumen. These implications are of significant importance for nutraceutical applications. Furthermore, these findings underscore the need for careful protein selection when interpreting protein-precipitation assays and for caution when extrapolating these results to animal or food systems.

4.4.5. Hydrolysable Tannin Assays

Hydrolysable tannins are commonly measured using the rhodanine assay, which detects gallic acid released after acid hydrolysis of gallotannins [142,155], or by quantifying ellagic acid after hydrolysis of ellagitannins via UV/DAD or LC methods [28,146]. These approaches are more specific for gallo- and ellagitannins than general phenolic assays, but they have notable limitations. Hydrolysis efficiency varies by matrix and tannin structure, leading to underestimation, while pre-existing free gallic or ellagic acid can inflate values unless blanks are included [155]. Harsh acid conditions can also degrade released products, and the assays only quantify released gallic or ellagic acid rather than capturing the structural diversity of intact hydrolysable tannins.

As emphasised in a review on hydrolysable tannin analysis in food by Arapitsas [156], the analytical challenge is compounded by the absence of commercially available hydrolysable tannin standards and by the sheer structural diversity of gallotannins and ellagitannins (molecular masses ~500–5000 Da, multiple galloyl/hexahydroxydiphenoyl (HHDP) substitution patterns). Historically, non-specific "total tannin" approaches based on absorbance at ~270 nm or the F–C reagent, as well as oxidant-based methods such as KIO_3^- and $NaNO_2$-reagent assays, have been used for hydrolysable tannin-rich foods, but

these are highly sensitive to oxygen, temperature and reaction time and provide, at best, semi-quantitative estimates [156]. Contemporary LC–DAD and LC–MS workflows increasingly quantify individual or grouped hydrolysable tannins as gallic acid, ellagic acid or isolated ellagitannin equivalents, yet still inherit uncertainties in extinction coefficients and ionisation efficiencies across different structures [156]. Collectively, these issues mean that colourimetric and hydrolysis-based hydrolysable tannin assays are best viewed as comparative or screening tools, and where hydrolysable tannins are central to nutraceutical claims, they should be complemented by structurally resolved methods (for example LC–MS/MS or NMR) to support more rigorous quantification and structure–activity interpretation.

4.4.6. Best Practice for Tannin Assays

All tannin assays are subject to extraction effects (solvent polarity, pH, antioxidants, oxidation artefacts, and matrix interferences from sugars, pigments, and metals) [13,157]. Results are also highly dependent on the choice of standard (e.g., catechin, tannic acid, cyanidin, phloroglucinol), which complicates cross-study comparison [141,157]. Colourimetric assays are biased toward monomers and oligomers, whereas protein-precipitation assays favour mid-DP polymers, leaving very high DP material under-represented [13,135]. To this effect, step-wise recommendations are listed below:

Step 1. Define the target

- Clearly specify whether the assay is intended to quantify condensed tannins (proanthocyanidins), hydrolysable tannins (e.g., gallotannins, ellagitannins), or protein-precipitable tannins (e.g., phlorotannins). Using "total tannins" without definition is misleading given the chemical heterogeneity and the different assay principles involved.

Step 2. Pair assays

- No single assay captures all tannin fractions. Pair methods to provide structural and functional balance—for example, butanol–HCl for estimating polymer content alongside DMACA for terminal units, or rhodanine/ellagic acid assays for hydrolysables. Cross-referencing assays allows identification of biases and a more nuanced interpretation of results.

Step 3. Pre-clean extracts

- Matrix constituents such as sugars, pigments, and organic acids can inflate absorbance values. Incorporating clean-up steps (e.g., polyvinylpolypyrrolidone (PVPP) treatment, solid-phase extraction (SPE), or differential solvent partitioning) reduces non-tannin interference and improves assay specificity.
- However, solvent-based clean-up steps can also strip tannins or selectively remove particular subfractions, especially lower-molecular-weight or more polar components [150]. Because these losses are often silent and assay-dependent, any solvent partitioning or back-extraction step should be validated for tannin retention rather than assumed to be chemically neutral. Similar caution applies to aggressive "clean-up" of bound-PA matrices using repeated organic extractions, which can alter the composition of the background and the inferred proportion of "insoluble" tannins [151].

Step 4. Report standards transparently

- Always justify the calibration standard used (catechin, epicatechin, cyanidin, tannic acid, etc.) and the chosen detection wavelength. Because extinction coefficients vary with subunit type, polymer length, and solvent system, calibration choices directly influence reported values and inter-study comparability.
- Optimisation work in *Leucaena* spp. demonstrated that antioxidants such as ascorbic acid or sodium metabisulphite and the presence or absence of Fe^{3+} can alter colour

yield by 20–60% and even change linearity ranges [150], highlighting the need to match antioxidant composition and reagent formulation between standards and samples.

Step 5. Complement with structural methods

- Where possible, supplement colourimetric or precipitation assays with structural analyses. Techniques such as LC-MS/MS, phloroglucinolysis, thiolysis, or MALDI-ToF can provide subunit composition, mean degree of polymerisation, and linkage information, enabling a mechanistic interpretation of assay outputs.

Step 6. Control oxidation

- Tannins are prone to oxidation, which alters polymer size and assay response. The use of antioxidants (e.g., ascorbic acid, sodium metabisulfite), low-temperature handling, and minimal exposure to prolonged heating or oxygen improves reproducibility and accuracy.

Step 7. Validate

- Apply spike–recovery experiments to confirm quantitative performance and test for completeness of hydrolysis in depolymerisation assays. Where possible, report conversion yields and discuss recovery rates, rather than assuming total conversion to reference chromophores.
- For bound or fibre-bound PA, validate the approach used for blank correction as well as the depolymerisation conditions. Comparative work in *Leucaena* spp. showed that simple heated aqueous blanks can substantially overestimate bound PA because they under-correct for co-extractable pigments, whereas unheated acidic blanks and wavelength-scanning methods with fitted baselines can recover added anthocyanidins much more accurately [153]. Incorporating such checks helps distinguish true bound PA from background colour.

Step 8. Contextualise claims

- Rather than treating a single "total tannin" number as definitive, interpret results in relation to functional behaviour. Protein-precipitation assays, for example, better reflect astringency and nutraceutical bioactivity than colourimetric equivalents alone. Integrating functional and structural data allows a more biologically meaningful assessment of tannin content.
- In addition, protein–tannin interactions are strongly influenced by protein identity, pH, and ionic environment. Assays that rely on a single model protein (e.g., BSA or gelatin) risk oversimplifying tannin reactivity, since different proteins exhibit selective affinities for tannins of varying size and structural motifs. Studies in diverse plant matrices show that physiologically relevant proteins bind tannins differently from BSA, and that some proteins form soluble rather than precipitable complexes [139]. Consequently, protein-precipitation assays should be interpreted as functional proxies rather than absolute measures of tannin concentration, and protein choice should be justified rather than assumed interchangeable.

4.4.7. Assay Selection Considerations for Tannin Analysis

Considering the structural heterogeneity of tannins and the diverse chemistries on which their assays are based, no universal "benchmark" conditions can be meaningfully summarised as was possible for TPC, TFC, and TMAC. Assay performance for tannins is inherently matrix-dependent, influenced by polymer size, subunit composition, galloylation, protein content, and co-extracted pigments or carbohydrates. Consequently, researchers should optimise assay parameters for their specific sample matrix or adopt protocols that have been explicitly validated for comparable materials.

Given this complexity, a more informative approach is to compare tannin assays according to their reaction mechanisms, tannin subclasses detected, susceptibility to matrix effects, and functional interpretability. This framework clarifies why different assays yield non-equivalent values across plant systems, and it supports more defensible assay selection aligned to analytical or nutraceutical objectives. Table 6 summarises these comparative attributes, highlighting the chemical basis, strengths, limitations, and appropriate use-cases for the principal tannin assay families.

Table 6. Comparative overview of major tannin assay chemistries, detectable tannin classes, and matrix sensitivities.

Assay	Underlying Chemical Principle	Tannin Subtypes Detected	Major Matrix Sensitivities/ Interferences	Strengths	Limitations/Cautions
Acid Butanol/ Porter Reaction	Acid-catalysed depolymerisation of PAs to carbocations conversion to anthocyanidins (coloured products)	Detects procyanidins; response increases with polymer length	Sugars and pigments (if not removed), heat-sensitive matrices, incomplete depolymerisation, differential yields between PC/PD units	Long-established method; semi-quantitative for DP; good for comparing samples within a single matrix	Incomplete conversion causes underestimation; PC vs. PD over-/under-response; requires heating; colour instability; not valid for phlorotannins or hydrolysables
Vanillin Assay	Aldehyde–phenol condensation with meta-dihydroxyl groups on the A-ring of flavan-3-ols	Reacts strongly with monomers; limited reactivity with PA extension units	Anthocyanins (absorb at 510 nm), chlorophyll, sugars; solvent effects (e.g., acetone quenching)	Simple; rapid; high sensitivity to catechin/epicatechin	Overestimates in pigmented matrices; poor for polymeric tannins; not specific across PA subtypes
DMACA Assay	Electrophilic aromatic substitution at C8 of terminal units forming a blue–green chromophore	Highly selective for terminal flavan-3-ols (catechin/epi), modest response to short oligomers	Water content (>1%), pH shifts, aldehyde stability, reagent degradation by light/heat	High specificity; minimal anthocyanin interference ($\lambda_{max} \approx 640$ nm); excellent for foods/beverages	Underestimates polymers; strongly dependent on reaction time, acidity, and reagent freshness
Protein Precipitation Assays	Quantification of tannin–protein insoluble complexes	Captures protein-reactive PAs; sensitive to polymer size, stereochemistry, galloylation	Protein source/type, pH, ionic strength, detergents, carbohydrates, polysaccharides	Physiologically relevant (astringency, digestibility); differentiates functional reactivity	Not strictly quantitative; different proteins give different results; reversible complexes often missed
Folin–Ciocalteu–based Tannin Indexes	Redox reaction with phenolic hydroxyls (not specific to tannins)	All phenolics including tannins	Sugars, ascorbate, reducing sugars, Maillard products	Works when PA-based assays are unsuitable; simple	Not tannin-specific; should only be used as a complementary index

PA = proanthocyanidin; PC = procyanidin; PD = prodelphinidin; DP = degree of polymerisation; DMACA = *p*-Dimethylaminocinnamaldehyde. Assays differ in chemical specificity, polymer-length sensitivity, and matrix-dependent reactivity; results are not directly comparable across methods and should be interpreted within the context of the analytical principle used.

5. Nutraceutical Workflows and Laboratory Pipelines for Industrial Use

Bridging analytical precision with commercial scalability is essential for transforming polyphenol-rich plant extracts into standardised nutraceutical products. Laboratory workflows must not only provide reliable quantification of bioactive compounds but also integrate decision-making logic that supports extraction optimisation, quality assurance, and regulatory compliance. Figure 12 summarises a practical workflow linking spectrophotometric assays with spectroscopic and chromatographic validation tools, illustrating how research laboratories can adapt these methods for industrial pipelines. The workflow begins with defining the analytical objective (screening versus purified fraction characterisation) and assessing whether the sample matrix is known. When phenolic pigments are detected, TPC is determined via the F–C assay, optionally accompanied by pigment correction for coloured matrices. Depending on analytical goals, the workflow branches into targeted assays: $AlCl_3$ for flavanols, $NaNO_2$–$AlCl_3$ for general flavonoids, and SBC for comprehensive subclass coverage. When blue–red–purple pigments dominate, the pH-differential TMAC assay quantifies anthocyanins. Samples exhibiting potential tannin activity progress to confirmatory assays—vanillin–HCl or DMACA for condensed tannins, rhodanine for hydrolysable tannins, and protein-precipitation for functional tannin capacity. Extracts

with minimal phenolic presence can be considered "Low Phenolic Content" and may not be worth extensive characterisation. Conversely, fractions demonstrating high absorbance or assay specificity are validated by LC–MS/MS or HPLC–DAD for structural confirmation. Complementary FTIR or NIR spectroscopy combined with chemometric modelling allows non-destructive, high-throughput authentication, enabling rapid feedback into extraction and formulation stages [51,158–160].

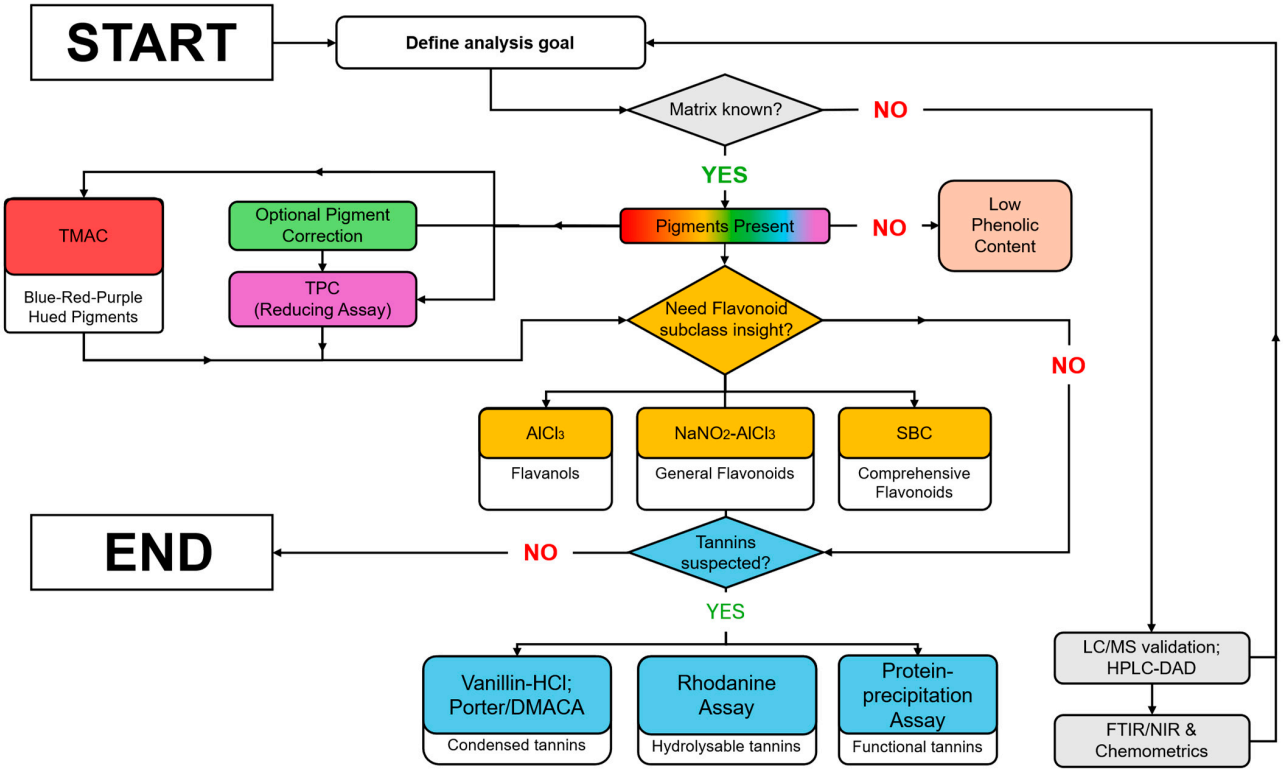


Figure 12. Workflow for nutraceutical analysis of polyphenol-rich plant extracts. Decision-tree outlining a practical laboratory pipeline for selecting appropriate spectrophotometric assays based on matrix properties, pigment content, and analytical objectives. The workflow guides users from initial assessment (matrix known/unknown, pigment presence, required subclass resolution) through targeted assays including TMAC (anthocyanins), TPC (reducing phenolics), $AlCl_3$, $NaNO_2$–$AlCl_3$, and SBC (flavonoids), and tannin-specific methods (vanillin–HCl, Porter/DMACA, rhodanine, and protein-precipitation assays). High-responding or structurally ambiguous samples proceed to confirmatory LC–MS/MS or HPLC–DAD, while FTIR/NIR combined with chemometrics enables rapid, non-destructive authentication suitable for industrial QC pipelines.

6. Conclusions

Spectrophotometric assays remain central to food and nutraceutical research because they are rapid, scalable, and cost-effective. Across the major classes of phenolic phytonutrient assays a consistent message emerges: the interpretive value of any colourimetric measurement depends far more on the clarity of the analytical question, the suitability of the assay chemistry, and the transparency of methodological reporting than on the assay itself. When these elements are misaligned, even well-designed experiments can generate misleading or incomparable outcomes.

Rather than viewing TPC, TFC, TMAC and tannin assays as stand-alone indicators, they are better understood as decision-support tools within a broader analytical pipeline. Each assay samples a specific subset of chemical behaviour such as reducing capacity, metal-complexation, pH-dependent chromophore formation, or depolymerisation, rather than quantifying a discrete compound class in a structural sense. When their chemical scope

is acknowledged explicitly, these methods can be strategically combined to characterise extracts, prioritise samples for further investigation, and guide more resource-intensive analyses such as LC–MS/MS and NIR/FTIR modelling.

A second theme for the appropriate application of colourimetric bench top assays is the importance of contextualisation. The concentration reported by a colourimetric assay has limited meaning in isolation; its value emerges when paired with clear calibration rationale, appropriate blanks, matrix controls, and validation steps that reflect the complexity of plant extracts. Whether the aim is to support quality assurance in industry, investigate phytochemical variation in plants, or assess nutraceutical potential, the defensibility of conclusions hinges on the rigour of these contextual controls and the alignment between assay chemistry and research question.

Moving forward, improving reproducibility across laboratories will depend on harmonised reporting standards, consistent use of matrix-matched calibrations, and greater adoption of hybrid workflows that integrate microplate colourimetry with spectroscopic or chromatographic confirmation. Well-designed ring trials would significantly advance consistency, helping to account for inter-laboratory variance and establish realistic benchmarks for comparative research.

Importantly, the role of colourimetric assays is evolving with increasing interest in high-throughput optimisation, flora cultivar screening, and natural-product development for food and cosmetic applications. When the results from these assays are transparently reported and complemented by structural datasets, they enable researchers to move from broad claims toward evidence-based evaluation of quality, authenticity, and functional potential.

Ultimately, colourimetric assays will continue to occupy a vital position in polyphenolic analysis. Their longevity is not a relic of convenience but a reflection of their unique analytical niche: simple, adaptable, insightful reactions that, when used with appropriate controls and clear chemical reasoning, provide reliable early-stage characterisation. By embracing their strengths, acknowledging their constraints, and embedding them within integrated analytical workflows, researchers can generate high-quality data that supports robust scientific interpretation and credible nutraceutical application.

Funding: This research received no external funding.

Institutional Review Board Statement: Not applicable.

Informed Consent Statement: Not applicable.

Data Availability Statement: No new data were created or analysed in this study. Data sharing is not applicable to this article.

Acknowledgments: Joseph Robert Nastasi acknowledges the support and encouragement of his colleagues and friends, including Cameron Shakes, Sudhanshu Pathania, and Robert Gargan, during the preparation of this review. Joseph Robert Nastasi would also like to acknowledge the help of Keely Rose Perry for assisting in making figure/graphics for this review.

Conflicts of Interest: The author declares no conflicts of interest.

Abbreviations

The following abbreviations are used in this manuscript:

AOAC	AOAC International (formerly Association of Official Analytical Chemists)
BSA	Bovine serum albumin
C3G	Cyanidin-3-O-glucoside

DAD	Diode-array detector
DEG	Diethylene glycol (in the DEG–NaOH assay)
DF	Dilution factor
DMACA	*p*-Dimethylaminocinnamaldehyde
DNPH	2,4-Dinitrophenylhydrazine
DP	Degree of polymerisation
ε	Molar extinction (absorptivity) coefficient
F–C	Folin–Ciocalteu (reagent/assay)
FW	Fresh weight
GAE	Gallic acid equivalents
HCl	Hydrochloric acid
HHDP	Hexahydroxydiphenoyl
HPLC	High-performance liquid chromatography
HPLC-DAD	High-performance liquid chromatography with diode-array detection
KOH	Potassium hydroxide
LC	Liquid chromatography
LC-MS/MS	Liquid chromatography–tandem mass spectrometry
λ_{max}	Wavelength of maximum absorbance
M3G	Malvidin-3-O-glucoside
MALDI-ToF	Matrix-assisted laser desorption/ionisation time-of-flight (mass spectrometry)
MW	Molecular weight
$NaNO_2$	Sodium nitrite
NaOH	Sodium hydroxide
Na_2CO_3	Sodium carbonate
NIR	Near-infrared (spectroscopy)
NMR	Nuclear magnetic resonance
PA	Proanthocyanidin
PVPP	Polyvinylpolypyrrolidone
R^2	Coefficient of determination
SBC	Sodium borohydride–chloranil (assay)
SPE	Solid-phase extraction
TFC	Total flavonoid content
TMAC	Total monomeric anthocyanin content
TPC	Total phenolic content
UV	Ultraviolet
UV–Vis	Ultraviolet–visible

References

1. Ashraf, M.A.; Iqbal, M.; Rasheed, R.; Hussain, I.; Riaz, M.; Arif, M.S. Environmental stress and secondary metabolites in plants: An overview. In *Plant Metabolites and Regulation Under Environmental Stress*; Academic Press: New York, NY, USA, 2018; pp. 153–167.
2. Chen, X.; Li, H.; Zhang, B.; Deng, Z. The synergistic and antagonistic antioxidant interactions of dietary phytochemical combinations. *Crit. Rev. Food Sci. Nutr.* **2022**, *62*, 5658–5677. [CrossRef]
3. Vignesh, A.; Amal, T.C.; Sarvalingam, A.; Vasanth, K. A review on the influence of nutraceuticals and functional foods on health. *Food Chem. Adv.* **2024**, *5*, 100749. [CrossRef]
4. McClements, D.J.; Decker, E.A.; Park, Y.; Weiss, J. Structural design principles for delivery of bioactive components in nutraceuticals and functional foods. *Crit. Rev. Food Sci. Nutr.* **2009**, *49*, 577–606. [CrossRef]
5. Wu, L.; Zhang, C.; Long, Y.; Chen, Q.; Zhang, W.; Liu, G. Food additives: From functions to analytical methods. *Crit. Rev. Food Sci. Nutr.* **2022**, *62*, 8497–8517. [CrossRef]
6. Delgado-Vargas, F.; Jiménez, A.; Paredes-López, O. Natural pigments: Carotenoids, anthocyanins, and betalains—Characteristics, biosynthesis, processing, and stability. *Crit. Rev. Food Sci. Nutr.* **2000**, *40*, 173–289. [CrossRef] [PubMed]
7. Sahebkar, A. Curcuminoids for the management of hypertriglyceridaemia. *Nat. Rev. Cardiol.* **2014**, *11*, 123. [CrossRef]

8. Saadati, F.; Chahardehi, A.M.; Jamshidi, N.; Jamshidi, N.; Ghasemi, D. Coumarin: A natural solution for alleviating inflammatory disorders. *Curr. Res. Pharmacol. Drug Discov.* **2024**, *7*, 100202. [CrossRef]
9. Scalbert, A.; Manach, C.; Morand, C.; Rémésy, C.; Jiménez, L. Dietary polyphenols and the prevention of diseases. *Crit. Rev. Food Sci. Nutr.* **2005**, *45*, 287–306. [CrossRef]
10. Mottaghi, S.; Abbaszadeh, H. A comprehensive mechanistic insight into the dietary and estrogenic lignans, arctigenin and sesamin as potential anticarcinogenic and anticancer agents. Current status, challenges, and future perspectives. *Crit. Rev. Food Sci. Nutr.* **2022**, *62*, 7301–7318. [CrossRef]
11. Oluwole, O.; Fernando, W.B.; Lumanlan, J.; Ademuyiwa, O.; Jayasena, V. Role of phenolic acid, tannins, stilbenes, lignans and flavonoids in human health—A review. *Int. J. Food Sci. Technol.* **2022**, *57*, 6326–6335. [CrossRef]
12. Catarino, M.D.; Silva, A.M.; Cardoso, S.M. Fucaceae: A source of bioactive phlorotannins. *Int. J. Mol. Sci.* **2017**, *18*, 1327. [CrossRef]
13. Hagerman, A. Tannin Handbook. 2002. Available online: https://sites.google.com/miamioh.edu/ann-hagerman-lab/tannin-handbook (accessed on 26 April 2025).
14. Chung, K.-T.; Wong, T.Y.; Wei, C.-I.; Huang, Y.-W.; Lin, Y. Tannins and human health: A review. *Crit. Rev. Food Sci. Nutr.* **1998**, *38*, 421–464. [CrossRef]
15. Granato, D.; Santos, J.S.; Maciel, L.G.; Nunes, D.S. Chemical perspective and criticism on selected analytical methods used to estimate the total content of phenolic compounds in food matrices. *TrAC Trends Anal. Chem.* **2016**, *80*, 266–279. [CrossRef]
16. El Darra, N.; Rajha, H.N.; Saleh, F.; Al-Oweini, R.; Maroun, R.G.; Louka, N. Food fraud detection in commercial pomegranate molasses syrups by UV–VIS spectroscopy, ATR-FTIR spectroscopy and HPLC methods. *Food Control* **2017**, *78*, 132–137. [CrossRef]
17. Penner, M.H. Ultraviolet, visible, and fluorescence spectroscopy. In *Food Analysis*; Springer International Publishing: Cham, Switzerland, 2017; pp. 89–106.
18. Shraim, A.M.; Ahmed, T.A.; Rahman, M.M.; Hijji, Y.M. Determination of total flavonoid content by aluminum chloride assay: A critical evaluation. *LWT* **2021**, *150*, 111932. [CrossRef]
19. Barreca, D.; Mandalari, G.; Calderaro, A.; Smeriglio, A.; Trombetta, D.; Felice, M.R.; Gattuso, G. Citrus flavones: An update on sources, biological functions, and health promoting properties. *Plants* **2020**, *9*, 288. [CrossRef]
20. Harborne, J.B.; Marby, H.; Marby, T. *The Flavonoids*; Springer: New York, NY, USA, 2013.
21. Harborne, J.B.; Mabry, T.J. *The Flavonoids: Advances in Research*, 1st ed.; Chapman and Hall Ltd.: London, UK, 1982.
22. Harborne, J.B. *The Flavonoids: Advances in Research Since 1980*; Springer: New York, NY, USA, 2013.
23. Gierschner, J.; Duroux, J.-L.; Trouillas, P. UV/Visible spectra of natural polyphenols: A time-dependent density functional theory study. *Food Chem.* **2012**, *131*, 79–89.
24. Kaeswurm, J.A.; Scharinger, A.; Teipel, J.; Buchweitz, M. Absorption coefficients of phenolic structures in different solvents routinely used for experiments. *Molecules* **2021**, *26*, 4656. [CrossRef]
25. Gould, K.; Davies, K.M.; Winefield, C. *Anthocyanins: Biosynthesis, Functions, and Applications*; Springer Science & Business Media: New York, NY, USA, 2009.
26. Charlton, N.C.; Mastyugin, M.; Török, B.; Török, M. Structural features of small molecule antioxidants and strategic modifications to improve potential bioactivity. *Molecules* **2023**, *28*, 1057. [CrossRef]
27. Porter, L.J.; Hrstich, L.N.; Chan, B.G. The conversion of procyanidins and prodelphinidins to cyanidin and delphinidin. *Phytochemistry* **1985**, *25*, 223–230. [CrossRef]
28. Quideau, S.; Deffieux, D.; Douat-Casassus, C.; Pouységu, L. Plant polyphenols: Chemical properties, biological activities, and synthesis. *Angew. Chem. Int. Ed.* **2011**, *50*, 586–621. [CrossRef]
29. Ford, L.; Theodoridou, K.; Sheldrake, G.N.; Walsh, P.J. A critical review of analytical methods used for the chemical characterisation and quantification of phlorotannin compounds in brown seaweeds. *Phytochem. Anal.* **2019**, *30*, 587–599. [CrossRef]
30. Macarrón, R.; Hertzberg, R.P. Design and implementation of high throughput screening assays. *Mol. Biotechnol.* **2011**, *47*, 270–285. [CrossRef]
31. Abderrahim, F.; Arribas, S.M.; Gonzalez, M.C.; Condezo-Hoyos, L. Rapid high-throughput assay to assess scavenging capacity index using DPPH. *Food Chem.* **2013**, *141*, 788–794. [CrossRef]
32. Huang, D.; Ou, B.; Hampsch-Woodill, M.; Flanagan, J.A.; Prior, R.L. High-throughput assay of oxygen radical absorbance capacity (ORAC) using a multichannel liquid handling system coupled with a microplate fluorescence reader in 96-well format. *J. Agric. Food Chem.* **2002**, *50*, 4437–4444. [CrossRef]
33. Lee, J.; Durst, R.W.; Wrolstad, R.E.; Collaborators. Determination of total monomeric anthocyanin pigment content of fruit juices, beverages, natural colorants, and wines by the pH differential method: Collaborative study. *J. AOAC Int.* **2005**, *88*, 1269–1278. [CrossRef]
34. Mayerhöfer, T.G.; Popp, J. Beer's law–why absorbance depends (almost) linearly on concentration. *ChemPhysChem* **2019**, *20*, 511–515. [CrossRef]

35. Henderson, T.; Nigam, P.S.; Owusu-Apenten, R.K. A universally calibrated microplate ferric reducing antioxidant power (FRAP) assay for foods and applications to Manuka honey. *Food Chem.* **2015**, *174*, 119–123. [CrossRef]
36. Auld, D.S.; Coassin, P.A.; Coussens, N.P.; Hensley, P.; Klumpp-Thomas, C.; Michael, S.; Sittampalam, G.S.; Trask, O.J.; Wagner, B.K.; Weidner, J.R. Microplate selection and recommended practices in high-throughput screening and quantitative biology. In *Assay Guidance Manual [Internet]*; National Institutes of Health: Bethesda, MD, USA, 2020.
37. Swinehart, D.F. The beer-lambert law. *J. Chem. Educ.* **1962**, *39*, 333. [CrossRef]
38. Mayerhöfer, T.G.; Mutschke, H.; Popp, J. Employing theories far beyond their limits—The case of the (Boguer-) beer–lambert law. *ChemPhysChem* **2016**, *17*, 1948–1955. [CrossRef]
39. Pérez, M.; Dominguez-López, I.; Lamuela-Raventós, R.M. The chemistry behind the folin–ciocalteu method for the estimation of (poly) phenol content in food: Total phenolic intake in a mediterranean dietary pattern. *J. Agric. Food Chem.* **2023**, *71*, 17543–17553. [CrossRef]
40. Galanakis, C.M. *Polyphenols: Properties, Recovery, and Applications*; Woodhead Publishing: Cambridge, UK, 2018.
41. Herrmann, K.M.; Weaver, L.M. The shikimate pathway. *Annu. Rev. Plant Biol.* **1999**, *50*, 473–503. [CrossRef]
42. Cassidy, A.; Hanley, B.; Lamuela-Raventos, R.M. Isoflavones, lignans and stilbenes–origins, metabolism and potential importance to human health. *J. Sci. Food Agric.* **2000**, *80*, 1044–1062. [CrossRef]
43. Rothwell, J.A.; Perez-Jimenez, J.; Neveu, V.; Medina-Remon, A.; M'hiri, N.; García-Lobato, P.; Manach, C.; Knox, C.; Eisner, R.; Wishart, D.S. Phenol-Explorer 3.0: A major update of the Phenol-Explorer database to incorporate data on the effects of food processing on polyphenol content. *Database* **2013**, *2013*, bat070. [CrossRef]
44. Folin, O.; Ciocalteu, V. On tyrosine and tryptophane determinations in proteins. *J. biol. Chem* **1927**, *73*, 627–650. [CrossRef]
45. Singleton, V.L.; Rossi, J.A. Colorimetry of total phenolics with phosphomolybdic-phosphotungstic acid reagents. *Am. J. Enol. Vitic.* **1965**, *16*, 144–158. [CrossRef]
46. Ainsworth, E.A.; Gillespie, K.M. Estimation of total phenolic content and other oxidation substrates in plant tissues using Folin–Ciocalteu reagent. *Nat. Protoc.* **2007**, *2*, 875–877. [CrossRef]
47. Everette, J.D.; Bryant, Q.M.; Green, A.M.; Abbey, Y.A.; Wangila, G.W.; Walker, R.B. Thorough study of reactivity of various compound classes toward the Folin− Ciocalteu reagent. *J. Agric. Food Chem.* **2010**, *58*, 8139–8144. [CrossRef]
48. Sánchez-Rangel, J.C.; Benavides, J.; Heredia, J.B.; Cisneros-Zevallos, L.; Jacobo-Velázquez, D.A. The Folin–Ciocalteu assay revisited: Improvement of its specificity for total phenolic content determination. *Anal. Methods* **2013**, *5*, 5990–5999. [CrossRef]
49. Motilva, M.-J.; Serra, A.; Macià, A. Analysis of food polyphenols by ultra high-performance liquid chromatography coupled to mass spectrometry: An overview. *J. Chromatogr. A* **2013**, *1292*, 66–82. [CrossRef]
50. Patle, T.K.; Shrivas, K.; Kurrey, R.; Upadhyay, S.; Jangde, R.; Chauhan, R. Phytochemical screening and determination of phenolics and flavonoids in Dillenia pentagyna using UV–vis and FTIR spectroscopy. *Spectrochim. Acta Part A Mol. Biomol. Spectrosc.* **2020**, *242*, 118717. [CrossRef]
51. Cozzolino, D. The role of visible and infrared spectroscopy combined with chemometrics to measure phenolic compounds in grape and wine samples. *Molecules* **2015**, *20*, 726–737. [CrossRef] [PubMed]
52. Kupina, S.; Fields, C.; Roman, M.C.; Brunelle, S.L. Determination of total phenolic content using the Folin-C assay: Single-laboratory validation, first action 2017.13. *J. AOAC Int.* **2018**, *101*, 1466–1472. [CrossRef]
53. Bobo-García, G.; Davidov-Pardo, G.; Arroqui, C.; Vírseda, P.; Marín-Arroyo, M.R.; Navarro, M. Intra-laboratory validation of microplate methods for total phenolic content and antioxidant activity on polyphenolic extracts, and comparison with conventional spectrophotometric methods. *J. Sci. Food Agric.* **2015**, *95*, 204–209. [CrossRef]
54. Andersen, O.M.; Markham, K.R. *Flavonoids: Chemistry, Biochemistry and Applications*; CRC Press: Boca Raton, FL, USA, 2005.
55. Panche, A.N.; Diwan, A.D.; Chandra, S.R. Flavonoids: An overview. *J. Nutr. Sci.* **2016**, *5*, e47. [CrossRef]
56. Barreca, D.; Trombetta, D.; Smeriglio, A.; Mandalari, G.; Romeo, O.; Felice, M.R.; Gattuso, G.; Nabavi, S.M. Food flavonols: Nutraceuticals with complex health benefits and functionalities. *Trends Food Sci. Technol.* **2021**, *117*, 194–204. [CrossRef]
57. Yang, X.; Jiang, Y.; Yang, J.; He, J.; Sun, J.; Chen, F.; Zhang, M.; Yang, B. Prenylated flavonoids, promising nutraceuticals with impressive biological activities. *Trends Food Sci. Technol.* **2015**, *44*, 93–104. [CrossRef]
58. Xiao, J. Dietary flavonoid aglycones and their glycosides: Which show better biological significance? *Crit. Rev. Food Sci. Nutr.* **2017**, *57*, 1874–1905. [CrossRef]
59. Chen, L.; Cao, H.; Huang, Q.; Xiao, J.; Teng, H. Absorption, metabolism and bioavailability of flavonoids: A review. *Crit. Rev. Food Sci. Nutr.* **2022**, *62*, 7730–7742. [CrossRef]
60. Sajeev, A.; Aswani, B.S.; Alqahtani, M.S.; Abbas, M.; Sethi, G.; Kunnumakkara, A.B. Harnessing Liquiritigenin: A Flavonoid-Based Approach for the Prevention and Treatment of Cancer. *Cancers* **2025**, *17*, 2328. [CrossRef] [PubMed]
61. Elbatreek, M.H.; Mahdi, I.; Ouchari, W.; Mahmoud, M.F.; Sobeh, M. Current advances on the therapeutic potential of pinocembrin: An updated review. *Biomed. Pharmacother.* **2023**, *157*, 114032. [CrossRef] [PubMed]
62. Xu, X.; Xie, H.; Hao, J.; Jiang, Y.; Wei, X. Flavonoid glycosides from the seeds of Litchi chinensis. *J. Agric. Food Chem.* **2011**, *59*, 1205–1209. [CrossRef]

63. Pyrzynska, K. Hesperidin: A review on extraction methods, stability and biological activities. *Nutrients* **2022**, *14*, 2387. [CrossRef]
64. Sun, Q.; Gao, S.; Yu, S.; Zheng, P.; Zhou, J. Production of (2S)-sakuranetin from (2S)-naringenin in Escherichia coli by strengthening methylation process and cell resistance. *Synth. Syst. Biotechnol.* **2022**, *7*, 1117–1125. [CrossRef] [PubMed]
65. Miyake, Y.; Yamamoto, K.; Osawa, T. Isolation of eriocitrin (eriodictyol 7-rutinoside) from lemon fruit (Citrus limon BURM. f.) and its antioxidative activity. *Food Sci. Technol. Int. Tokyo* **1997**, *3*, 84–89. [CrossRef]
66. Gattuso, G.; Barreca, D.; Gargiulli, C.; Leuzzi, U.; Caristi, C. Flavonoid composition of citrus juices. *Molecules* **2007**, *12*, 1641–1673. [CrossRef] [PubMed]
67. Allemailem, K.S.; Almatroudi, A.; Alharbi, H.O.A.; AlSuhaymi, N.; Alsugoor, M.H.; Aldakheel, F.M.; Khan, A.A.; Rahmani, A.H. Apigenin: A bioflavonoid with a promising role in disease prevention and treatment. *Biomedicines* **2024**, *12*, 1353. [CrossRef]
68. Almatroodi, S.A.; Almatroudi, A.; Alharbi, H.O.A.; Khan, A.A.; Rahmani, A.H. Effects and mechanisms of luteolin, a plant-based flavonoid, in the prevention of cancers via modulation of inflammation and cell signaling molecules. *Molecules* **2024**, *29*, 1093. [CrossRef]
69. Singh, A.; Kumar, V. Nutritional, phytochemical, and antimicrobial attributes of seeds and kernels of different pumpkin cultivars. *Food Front.* **2022**, *3*, 182–193. [CrossRef]
70. Capó, X.; Kumar, R.; Mishra, A.P.; Nigam, M.; Waranuch, N.; Martorell, M.; Sharopov, F.; Calina, D.; Popa, D.; Setzer, W.N. Baicalein and baicalin in cancer therapy: Multifaceted mechanisms, preclinical evidence, and translational challenges. In *Seminars in Oncology*; W. B. Saunders: Philadelphia, PA, USA, 2025; p. 152377.
71. Gao, S.; Siddiqui, N.; Etim, I.; Du, T.; Zhang, Y.; Liang, D. Developing nutritional component chrysin as a therapeutic agent: Bioavailability and pharmacokinetics consideration, and ADME mechanisms. *Biomed. Pharmacother.* **2021**, *142*, 112080. [CrossRef]
72. Zhou, Z.; Li, T.; Qin, H.; Wang, X.; He, S.; Fan, Z.; Ye, Q.; Du, Y. Acacetin as a natural cardiovascular therapeutic: Mechanisms and preclinical evidence. *Front. Pharmacol.* **2025**, *16*, 1493981. [CrossRef]
73. Heo, M.Y.; Sohn, S.J.; Au, W.W. Anti-genotoxicity of galangin as a cancer chemopreventive agent candidate. *Mutat. Res./Rev. Mutat. Res.* **2001**, *488*, 135–150. [CrossRef] [PubMed]
74. Bentz, A.B. A Review of quercetin: Chemistry, antioxident properties, and bioavailability. *J. Young Investig.* **2009**.
75. Khoo, C.; Falk, M. Cranberry polyphenols: Effects on cardiovascular risk factors. In *Polyphenols in Human Health and Disease*; Elsevier: Amsterdam, The Netherlands, 2014; pp. 1049–1065.
76. Dabeek, W.M.; Marra, M.V. Dietary quercetin and kaempferol: Bioavailability and potential cardiovascular-related bioactivity in humans. *Nutrients* **2019**, *11*, 2288. [CrossRef]
77. Park, K.-S.; Chong, Y.; Kim, M.K. Myricetin: Biological activity related to human health. *Appl. Biol. Chem.* **2016**, *59*, 259–269. [CrossRef]
78. Sinha, K.; Ghosh, J.; Sil, P.C. Morin and its role in chronic diseases. In *Anti-Inflammatory Nutraceuticals and Chronic Diseases*; Springer: New York, NY, USA, 2016; pp. 453–471.
79. Rajput, S.A.; Wang, X.-Q.; Yan, H.-C. Morin hydrate: A comprehensive review on novel natural dietary bioactive compound with versatile biological and pharmacological potential. *Biomed. Pharmacother.* **2021**, *138*, 111511. [CrossRef]
80. Szymczak, J.; Cielecka-Piontek, J. Fisetin—In search of better bioavailability—From macro to nano modifications: A review. *Int. J. Mol. Sci.* **2023**, *24*, 14158. [CrossRef] [PubMed]
81. Yin, C.; Han, S.; Fang, X.; Jin, C.; Han, B.; Wang, M. Insight into the flavor characteristics and antioxidant activity in Xiaoqinggan black tea. *Food Res. Int.* **2025**, *221*, 117227. [CrossRef]
82. Sunil, C.; Xu, B. An insight into the health-promoting effects of taxifolin (dihydroquercetin). *Phytochemistry* **2019**, *166*, 112066. [CrossRef]
83. Chen, J.; Wang, X.; Xia, T.; Bi, Y.; Liu, B.; Fu, J.; Zhu, R. Molecular mechanisms and therapeutic implications of dihydromyricetin in liver disease. *Biomed. Pharmacother.* **2021**, *142*, 111927. [CrossRef]
84. Kim, T.; Kwon, Y.E.; Park, S.M.; Kim, M.S.; Jeong, Y.H.; Park, S.Y.; Bae, Y.-S.; Cheong, E.J.; He, Y.-C.; Gong, C. Chemotaxonomic significance of taxifolin-3-O-arabinopyranoside in Rhododendron species native to Korea. *J. For. Environ. Sci.* **2022**, *38*, 159–173.
85. El-Shiekh, R.A.; Radi, M.H.; Abdel-Sattar, E. Unveiling the therapeutic potential of aromadendrin (AMD): A promising anti-inflammatory agent in the prevention of chronic diseases. *Inflammopharmacology* **2025**, *33*, 1209–1220. [CrossRef] [PubMed]
86. Sharma, A.; Gupta, S.; Chauhan, S.; Nair, A.; Sharma, P. Astilbin: A promising unexplored compound with multidimensional medicinal and health benefits. *Pharmacol. Res.* **2020**, *158*, 104894. [CrossRef]
87. Coutinho-Wolino, K.S.; Almeida, P.P.; Mafra, D.; Stockler-Pinto, M.B. Bioactive compounds modulating Toll-like 4 receptor (TLR4)-mediated inflammation: Pathways involved and future perspectives. *Nutr. Res.* **2022**, *107*, 96–116. [CrossRef]
88. Prakash, M.; Basavaraj, B.; Murthy, K.C. Biological functions of epicatechin: Plant cell to human cell health. *J. Funct. Foods* **2019**, *52*, 14–24. [CrossRef]
89. Ntamo, Y.; Jack, B.; Ziqubu, K.; Mazibuko-Mbeje, S.E.; Nkambule, B.B.; Nyambuya, T.M.; Mabhida, S.E.; Hanser, S.; Orlando, P.; Tiano, L. Epigallocatechin gallate as a nutraceutical to potentially target the metabolic syndrome: Novel insights into therapeutic effects beyond its antioxidant and anti-inflammatory properties. *Crit. Rev. Food Sci. Nutr.* **2024**, *64*, 87–109. [CrossRef]

90. Wani, S.M.; Hussain, P.R.; Masoodi, F.A.; Ahmad, M.; Wani, T.A.; Gani, A.; Rather, S.A.; Suradkar, P. Evaluation of the composition of bioactive compounds and antioxidant activity in fourteen apricot varieties of North India. *J. Agric. Sci.* **2017**, *9*, 66–82. [CrossRef]
91. Toshima, S.; Hirano, T.; Kunitake, H. Comparison of anthocyanins, polyphenols, and antioxidant capacities among raspberry, blackberry, and Japanese wild Rubus species. *Sci. Hortic.* **2021**, *285*, 110204. [CrossRef]
92. Johnson, R.; Bryant, S.; Huntley, A.L. Green tea and green tea catechin extracts: An overview of the clinical evidence. *Maturitas* **2012**, *73*, 280–287. [CrossRef]
93. Ganai, A.A.; Farooqi, H. Bioactivity of genistein: A review of in vitro and in vivo studies. *Biomed. Pharmacother.* **2015**, *76*, 30–38. [CrossRef]
94. Miller, K.A.; Frankel, F.; Takahashr, H.; Vance, N.; Stiegerwald, C.; Edelstein, S. Collected literature on isoflavones and chronic diseases. *Cogent Food Agric.* **2016**, *2*, 1135861. [CrossRef]
95. Xuan, T.; Liu, Y.; Liu, R.; Liu, S.; Han, J.; Bai, X.; Wu, J.; Fan, R. Advances in extraction, purification, and analysis techniques of the main components of kudzu root: A comprehensive review. *Molecules* **2023**, *28*, 6577. [CrossRef]
96. Jackson, C.-J.; Dini, J.; Lavandier, C.; Rupasinghe, H.; Faulkner, H.; Poysa, V.; Buzzell, D.; DeGrandis, S. Effects of processing on the content and composition of isoflavones during manufacturing of soy beverage and tofu. *Process Biochem.* **2002**, *37*, 1117–1123. [CrossRef]
97. Mu, H.; Bai, Y.-H.; Wang, S.-T.; Zhu, Z.-M.; Zhang, Y.-W. Research on antioxidant effects and estrogenic effect of formononetin from Trifolium pratense (red clover). *Phytomedicine* **2009**, *16*, 314–319. [CrossRef]
98. Xie, J.; Zhang, Y.; Wang, W.; Hou, J. Identification and simultaneous determination of glycyrrhizin, formononetin, glycyrrhetinic acid, liquiritin, isoliquiritigenin, and licochalcone A in licorice by LC-MS/MS. *Acta Chromatogr.* **2014**, *26*, 507–516. [CrossRef]
99. Zhang, J.; Liu, L.; Wang, J.; Ren, B.; Zhang, L.; Li, W. Formononetin, an isoflavone from Astragalus membranaceus inhibits proliferation and metastasis of ovarian cancer cells. *J. Ethnopharmacol.* **2018**, *221*, 91–99. [CrossRef]
100. Kao, T.H.; Lu, Y.F.; Hsieh, H.C.; Chen, B.H. Stability of isoflavone glucosides during processing of soymilk and tofu. *Food Res. Int.* **2004**, *37*, 891–900. [CrossRef]
101. Feng, Z.-J.; Lai, W.-F. Chemical and biological properties of biochanin A and its pharmaceutical applications. *Pharmaceutics* **2023**, *15*, 1105. [CrossRef]
102. Christ, B.; Müller, K. Zur serienmäßigen Bestimmung des Gehaltes an Flavonol-Derivaten in Drogen. *Arch. Der Pharm.* **1960**, *293*, 1033–1042. [CrossRef]
103. Barnum, D.W. Spectrophotometric determination of catechol, epinephrine, dopa, dopamine and other aromatic vic-diols. *Anal. Chim. Acta* **1977**, *89*, 157–166. [CrossRef]
104. Zhishen, J.; Mengcheng, T.; Jianming, W. The determination of flavonoid contents in mulberry and their scavenging effects on superoxide radicals. *Food Chem.* **1999**, *64*, 555–559. [CrossRef]
105. Pękal, A.; Pyrzynska, K. Evaluation of aluminium complexation reaction for flavonoid content assay. *Food Anal. Methods* **2014**, *7*, 1776–1782. [CrossRef]
106. Sultana, S.; Lawag, I.L.; Lim, L.Y.; Foster, K.J.; Locher, C. A Critical Exploration of the Total Flavonoid Content Assay for Honey. *Methods Protoc.* **2024**, *7*, 95. [CrossRef]
107. Nicolescu, A.; Bunea, C.I.; Mocan, A. Total flavonoid content revised: An overview of past, present, and future determinations in phytochemical analysis. *Anal. Biochem.* **2025**, *700*, 115794. [CrossRef]
108. He, X.; Liu, D.; Liu, R.H. Sodium borohydride/chloranil-based assay for quantifying total flavonoids. *J. Agric. Food Chem.* **2008**, *56*, 9337–9344. [CrossRef] [PubMed]
109. Sedgwick, P. Pearson's correlation coefficient. *BMJ* **2012**, *345*, e4483. [CrossRef]
110. Rolim, A.; Maciel, C.P.; Kaneko, T.M.; Consiglieri, V.O.; Salgado-Santos, I.M.; Velasco, M.V.R. Validation assay for total flavonoids, as rutin equivalents, from Trichilia catigua Adr. Juss (Meliaceae) and Ptychopetalum olacoides Bentham (Olacaceae) commercial extract. *J. AOAC Int.* **2005**, *88*, 1015–1019. [CrossRef] [PubMed]
111. de Villiers, A.; Venter, P.; Pasch, H. Recent advances and trends in the liquid-chromatography–mass spectrometry analysis of flavonoids. *J. Chromatogr. A* **2016**, *1430*, 16–78. [CrossRef]
112. Huang, R.; Wu, W.; Shen, S.; Fan, J.; Chang, Y.; Chen, S.; Ye, X. Evaluation of colorimetric methods for quantification of citrus flavonoids to avoid misuse. *Anal. Methods* **2018**, *10*, 2575–2587. [CrossRef]
113. Nagy, M.; Grančai, D. Colorimetric determination of flavanones in propolis. *Pharmazie* **1996**, *51*, 100–101.
114. Kim, G.-N.; Shin, M.-R.; Shin, S.H.; Lee, A.R.; Lee, J.Y.; Seo, B.-I.; Kim, M.Y.; Kim, T.H.; Noh, J.S.; Rhee, M.H. Study of antiobesity effect through inhibition of pancreatic lipase activity of Diospyros kaki fruit and Citrus unshiu peel. *BioMed Res. Int.* **2016**, *2016*, 1723042. [CrossRef]
115. Li, Y.G.; Tanner, G.; Larkin, P. The DMACA–HCl protocol and the threshold proanthocyanidin content for bloat safety in forage legumes. *J. Sci. Food Agric.* **1996**, *70*, 89–101. [CrossRef]

116. Matić, P.; Sabljić, M.; Jakobek, L. Validation of spectrophotometric methods for the determination of total polyphenol and total flavonoid content. *J. AOAC Int.* **2017**, *100*, 1795–1803. [CrossRef] [PubMed]
117. Herald, T.J.; Gadgil, P.; Tilley, M. High-throughput micro plate assays for screening flavonoid content and DPPH-scavenging activity in sorghum bran and flour. *J. Sci. Food Agric.* **2012**, *92*, 2326–2331. [CrossRef]
118. Sondheimer, E.; Kertesz, Z. The Anthocyanin of Strawberries [1]. *J. Am. Chem. Soc.* **1948**, *70*, 3476–3479. [CrossRef] [PubMed]
119. Rapisarda, P.; Fanella, F.; Maccarone, E. Reliability of analytical methods for determining anthocyanins in blood orange juices. *J. Agric. Food Chem.* **2000**, *48*, 2249–2252. [CrossRef]
120. Lee, J.; Rennaker, C.; Wrolstad, R.E. Correlation of two anthocyanin quantification methods: HPLC and spectrophotometric methods. *Food Chem.* **2008**, *110*, 782–786. [CrossRef]
121. Hay, T.O.; Fitzgerald, M.A.; Nastasi, J.R. Systematic application of UPLC-Q-ToF-MS/MS coupled with chemometrics for the identification of natural food pigments from Davidson plum and native currant. *Food Chem. X* **2025**, *25*, 102072. [CrossRef]
122. Lee, J.; Durst, R.; Wrolstad, R. AOAC official method 2005.02: Total monomeric anthocyanin pigment content of fruit juices, beverages, natural colorants, and wines by the pH differential method. *Off. Methods Anal. AOAC Int.* **2005**, *2*.
123. Liu, Y.; Zhang, Y.; Zhou, Y.; Feng, X.-S. Anthocyanins in different food matrices: Recent updates on extraction, purification and analysis techniques. *Crit. Rev. Anal. Chem.* **2024**, *54*, 1430–1461. [CrossRef]
124. Castañeda-Ovando, A.; de Lourdes Pacheco-Hernández, M.; Páez-Hernández, M.E.; Rodríguez, J.A.; Galán-Vidal, C.A. Chemical studies of anthocyanins: A review. *Food Chem.* **2009**, *113*, 859–871. [CrossRef]
125. Rodriguez-Amaya, D.B. Update on natural food pigments—A mini-review on carotenoids, anthocyanins, and betalains. *Food Res. Int.* **2019**, *124*, 200–205. [CrossRef]
126. Giusti, M.M.; Rodríguez-Saona, L.E.; Wrolstad, R.E. Molar absorptivity and color characteristics of acylated and non-acylated pelargonidin-based anthocyanins. *J. Agric. Food Chem.* **1999**, *47*, 4631–4637. [CrossRef] [PubMed]
127. Jordheim, M.; Aaby, K.; Fossen, T.; Skrede, G.; Andersen, Ø.M. Molar absorptivities and reducing capacity of pyranoanthocyanins and other anthocyanins. *J. Agric. Food Chem.* **2007**, *55*, 10591–10598. [CrossRef] [PubMed]
128. Singh, M.C.; Price, W.E.; Kelso, C.; Charlton, K.; Probst, Y. Impact of molar absorbance on anthocyanin content of the foods. *Food Chem.* **2022**, *386*, 132855. [CrossRef]
129. Mohammadi, N.; Farrell, M.; O'Sullivan, L.; Langan, A.; Franchin, M.; Azevedo, L.; Granato, D. Effectiveness of anthocyanin-containing foods and nutraceuticals in mitigating oxidative stress, inflammation, and cardiovascular health-related biomarkers: A systematic review of animal and human interventions. *Food Funct.* **2024**, *15*, 3274–3299. [CrossRef]
130. Harvey, D. *Modern Analytical Chemistry*; McGraw Hill: New York, NY, USA, 2000.
131. Gündüz, K.; Serçe, S.; Hancock, J.F. Variation among highbush and rabbiteye cultivars of blueberry for fruit quality and phytochemical characteristics. *J. Food Compos. Anal.* **2015**, *38*, 69–79. [CrossRef]
132. Ali, A.; Cottrell, J.J.; Dunshea, F.R. Identification and characterization of anthocyanins and non-anthocyanin phenolics from Australian native fruits and their antioxidant, antidiabetic, and anti-Alzheimer potential. *Food Res. Int.* **2022**, *162*, 111951. [CrossRef] [PubMed]
133. Cabrita, L.; Fossen, T.; Andersen, Ø.M. Colour and stability of the six common anthocyanidin 3-glucosides in aqueous solutions. *Food Chem.* **2000**, *68*, 101–107. [CrossRef]
134. Harbertson, J.F.; Picciotto, E.A.; Adams, D.O. Measurement of polymeric pigments in grape berry extract sand wines using a protein precipitation assay combined with bisulfite bleaching. *Am. J. Enol. Vitic.* **2003**, *54*, 301–306. [CrossRef]
135. Hagerman, A.E.; Butler, L.G. The specificity of proanthocyanidin-protein interactions. *J. Biol. Chem.* **1981**, *256*, 4494–4497. [CrossRef]
136. Ottaviani, J.I.; Kwik-Uribe, C.; Keen, C.L.; Schroeter, H. Intake of dietary procyanidins does not contribute to the pool of circulating flavanols in humans. *Am. J. Clin. Nutr.* **2012**, *95*, 851–858. [CrossRef]
137. Espín, J.C.; Larrosa, M.; García-Conesa, M.T.; Tomás-Barberán, F. Biological significance of urolithins, the gut microbial ellagic acid-derived metabolites: The evidence so far. *Evid.-Based Complement. Altern. Med.* **2013**, *2013*, 270418. [CrossRef] [PubMed]
138. Murray, M.; Dordevic, A.L.; Ryan, L.; Bonham, M.P. An emerging trend in functional foods for the prevention of cardiovascular disease and diabetes: Marine algal polyphenols. *Crit. Rev. Food Sci. Nutr.* **2018**, *58*, 1342–1358. [CrossRef] [PubMed]
139. Perez-Maldonado, R.A.; Norton, B.W.; Kerven, G.L. Factors affecting in vitro formation of tannin-protein complexes. *J. Sci. Food Agric.* **1995**, *69*, 291–298. [CrossRef]
140. Folin, O.; Denis, W. On phosphotungstic-phosphomolybdic compounds as color reagents. *J. Biol. Chem.* **1912**, *12*, 239–243. [CrossRef]
141. Price, M.L.; Van Scoyoc, S.; Butler, L.G. A critical evaluation of the vanillin reaction as an assay for tannin in sorghum grain. *J. Agric. Food Chem.* **1978**, *26*, 1214–1218. [CrossRef]
142. Inoue, K.H.; Hagerman, A.E. Determination of gallotannin with rhodanine. *Anal. Biochem.* **1988**, *169*, 363–369. [CrossRef] [PubMed]

143. Broadhurst, R.B.; Jones, W.T. Analysis of condensed tannins using acidified vanillin. *J. Sci. Food Agric.* **1978**, *29*, 788–794. [CrossRef]
144. Sun, B.; Ricardo-da-Silva, J.M.; Spranger, I. Critical factors of vanillin assay for catechins and proanthocyanidins. *J. Agric. Food Chem.* **1998**, *46*, 4267–4274. [CrossRef]
145. Khoshayand, M.R.; Roohi, T.; Moghaddam, G.; Khoshayand, F.; Shahbazikhah, P.; Oveisi, M.R.; Hajimahmoodi, M. Optimization of a vanillin assay for determination of anthocyanins using D-optimal design. *Anal. Methods* **2012**, *4*, 824–829. [CrossRef]
146. Waterman, P.G.; Mole, S. *Analysis of Phenolic Plant Metabolites*; Blackwell Scientific Publications: Oxford, UK, 1994.
147. Gessner, M.O.; Steiner, D. Acid butanol assay for proanthocyanidins (condensed tannins). In *Methods to Study Litter Decomposition: A Practical Guide*; Springer: New York, NY, USA, 2005; pp. 107–114.
148. Makkar, H.P.; Gamble, G.; Becker, K. Limitation of the butanol–hydrochloric acid–iron assay for bound condensed tannins. *Food Chem.* **1999**, *66*, 129–133. [CrossRef]
149. Shay, P.-E.; Trofymow, J.; Constabel, C.P. An improved butanol-HCl assay for quantification of water-soluble, acetone: Methanol-soluble, and insoluble proanthocyanidins (condensed tannins). *Plant Methods* **2017**, *13*, 63. [CrossRef]
150. Dalzell, S.A.; Kerven, G.L. A rapid method for the measurement of *Leucaena* spp. proanthocyanidins by the proanthocyanidin (butanol/HCl) assay. *J. Sci. Food Agric.* **1998**, *78*, 405–416. [CrossRef]
151. Dalzell, S.A.; Kerven, G.L. Accounting for co-extractable compounds (blank correction) in spectrophotometric measurement of extractable and total-bound proanthocyanidin in *Leucaena* spp. *J. Sci. Food Agric.* **2002**, *82*, 860–868. [CrossRef]
152. Wallace, T.C.; Giusti, M.M. Evaluation of parameters that affect the 4-dimethylaminocinnamaldehyde assay for flavanols and proanthocyanidins. *J. Food Sci.* **2010**, *75*, C619–C625. [CrossRef] [PubMed]
153. Hagerman, A.E.; Butler, L.G. Protein precipitation method for the quantitative determination of tannins. *J. Agric. Food Chem.* **1978**, *26*, 809–812. [CrossRef]
154. Sarneckis, C.J.; Dambergs, R.; Jones, P.; Mercurio, M.; Herderich, M.J.; Smith, P. Quantification of condensed tannins by precipitation with methyl cellulose: Development and validation of an optimised tool for grape and wine analysis. *Aust. J. Grape Wine Res.* **2006**, *12*, 39–49. [CrossRef]
155. Willis, R. Improved method for measuring hydrolyzable tannins using potassium iodate. *Analyst* **1998**, *123*, 435–439. [CrossRef]
156. Arapitsas, P. Hydrolyzable tannin analysis in food. *Food Chem.* **2012**, *135*, 1708–1717. [CrossRef]
157. Kennedy, J.A.; Jones, G.P. Analysis of proanthocyanidin cleavage products following acid-catalysis in the presence of excess phloroglucinol. *J. Agric. Food Chem.* **2001**, *49*, 1740–1746. [CrossRef] [PubMed]
158. Cozzolino, D. Infrared methods for high throughput screening of metabolites: Food and medical applications. *Comb. Chem. High Throughput Screen.* **2011**, *14*, 125–131. [CrossRef]
159. Cozzolino, D. Infrared spectroscopy as a versatile analytical tool for the quantitative determination of antioxidants in agricultural products, foods and plants. *Antioxidants* **2015**, *4*, 482–497. [CrossRef] [PubMed]
160. Cozzolino, D. An overview of the successful application of vibrational spectroscopy techniques to quantify nutraceuticals in fruits and plants. *Foods* **2022**, *11*, 315. [CrossRef] [PubMed]

Disclaimer/Publisher's Note: The statements, opinions and data contained in all publications are solely those of the individual author(s) and contributor(s) and not of MDPI and/or the editor(s). MDPI and/or the editor(s) disclaim responsibility for any injury to people or property resulting from any ideas, methods, instructions or products referred to in the content.